

A STOCHASTIC MODEL FOR THE LUMINOSITY FLUCTUATIONS OF ACCRETING BLACK HOLES

BRANDON C. KELLY^{1,2,3}, MAŁGORZATA SOBOLEWSKA³, ANETA SIEMIGINOWSKA³*Draft version May 23, 2018*

ABSTRACT

In this work we have developed a new stochastic model for the fluctuations in lightcurves of accreting black holes. The model is based on a linear combination of stochastic processes and is also the solution to the linear diffusion equation perturbed by a spatially correlated noise field. This allows flexible modeling of the power spectral density (PSD), and we derive the likelihood function for the process, enabling one to estimate the parameters of the process, including break frequencies in the PSD. Our statistical technique is computationally efficient, unbiased by aliasing and red noise leak, and fully accounts for irregular sampling and measurement errors. We show that our stochastic model provides a good approximation to the X-ray lightcurves of galactic black holes, and the optical and X-ray lightcurves of AGN. We use the estimated time scales of our stochastic model to recover the correlation between characteristic time scale of the high frequency X-ray fluctuations and black hole mass for AGN, including two new ‘detections’ of the time scale for Fairall 9 and NGC 5548. We find a tight anti-correlation between the black hole mass and the amplitude of the driving noise field, which is proportional to the amplitude of the high frequency X-ray PSD, and we estimate that this parameter gives black hole mass estimates to within ~ 0.2 dex precision, potentially the most accurate method for AGN yet. We also find evidence that $\approx 13\%$ of AGN optical PSDs fall off flatter than $1/f^2$, and, similar to previous work, find that the optical fluctuations are more suppressed on short time scales compared to the X-rays, but are larger on long time scales, suggesting the optical fluctuations are not solely due to reprocessing of X-rays.

Subject headings: accretion, accretion disks — galaxies: active — methods: data analysis — quasars: general

1. INTRODUCTION

Both galactic black holes (GBH) and active galactic nuclei (AGN), being black hole accretion systems, share a number of similarities in their spectroscopic and variability features despite being separated by several decades in mass. The major ingredients of the two systems appear to be an optically thick, geometrically thin accretion disk emitting thermal radiation, and an optically thin hot ‘corona’ emitting X-ray emission with a power-law spectrum. Because the temperature of the disk scales with the black hole mass as $kT \propto M_{BH}^{-1/4}$, the thermal disk emits in the soft X-rays for GBHs, and in the optical/UV region for AGN. The source and geometry of the corona emission is not known, but likely involves inverse compton emission from a hot electron plasma (e.g., Shapiro et al. 1976; Haardt & Maraschi 1991) with a possible synchrotron contribution from a jet (Markoff et al. 2001, 2005). Both GBHs and AGN follow a correlation between the black hole mass, radio luminosity, and X-ray luminosity (Merloni et al. 2003; Kōrding et al. 2006; Yuan et al. 2009; Gültekin et al. 2009b), leading some to suggest that the systems are largely self-similar, at least in low accretion rate states, differing only in mass and environment (e.g., Falcke et al. 2004).

However, the comparison between GBHs and AGNs is not straightforward, as GBHs are known to exist in different ‘states’, with the same source seen

cycling between the various states (for a review see Remillard & McClintock 2006; Belloni 2010). The spectral and timing properties of GBHs are different in the different states. The most commonly observed states are the hard, soft, and very high state (VHS). In the hard state, the spectrum is dominated by the power-law hard X-ray emission, while in the soft state the X-ray flux increases and the spectrum contains a significant thermal disk component. In the VHS, the X-ray flux is very high and the spectrum is intermediate in hardness between the soft and hard states. The power spectral density (PSD, $P(f)$) of the X-ray fluctuations can be reasonably approximated by bending power-laws, $P(f) \propto 1/f^\alpha$. For the soft and intermediate states, the power-law component contributes to the majority of the variability (e.g., Done & Gierliński 2005; Sobolewska & Życki 2006), while for the hard state the disk blackbody component dominates the soft X-ray variability, at least on time scales > 1 sec (Wilkinson & Uttley 2009). The PSD at high frequencies has a logarithmic slope $\alpha \gtrsim 2$, flattening to a slope of $\alpha \sim 1$ below some break frequency. For GBH in the hard state and VHS, there is an additional flattening to $\alpha = 0$ below a second lower break frequency, with the break frequencies being higher in the VHS. The accretion rate increases as one moves from the hard state to the VHS.

For AGN the situation is less clear, due to the fact that the time scales involved for the state transitions are expected to scale upwards with black hole mass. As such, AGN, with their supermassive black holes (SMBH), have not been observed to unambiguously undergo state transitions. Many AGN display SEDs

¹ bckelly@cfa.harvard.edu² Hubble Fellow³ Harvard-Smithsonian Center for Astrophysics, 60 Garden St, Cambridge, MA 02138

more characteristic of soft state GBH, in that there is a strong thermal component from the disk in the optical/UV region. Sobolewska et al. (2009) suggest, based on comparisons of the AGN and GBH SEDs, that most AGN in current surveys are in the VHS (see also Sobolewska, Siemiginowska, & Gierlinsky 2011). Almost all of the ~ 10 AGN with high quality X-ray lightcurves exhibit PSDs similar to those seen in Cyg X-1 in the soft state (e.g., Markowitz et al. 2003; McHardy et al. 2006). The only exception is Akn 564, which exhibits a second low-frequency break (Arévalo et al. 2006; McHardy et al. 2007). The high accretion rate ($\dot{m} \sim 1$, Romano et al. 2004) led McHardy et al. (2007) to suggest that this source is analogous to the VHS. However, the average 2–10 keV photon index of these sources is $\Gamma < 2$ (Papadakis et al. 2009; Sobolewska & Papadakis 2009), which resembles the value observed for GBHs in the hard state; thus, there is some discrepancy between the spectral and timing classifications. The break frequencies for both GBHs and AGN are observed to anti-correlate with black hole mass (Uttley & McHardy 2005; McHardy et al. 2006), further strengthening the similarity between GBHs and AGN. The anti-correlation between the break frequency and black hole mass has typically been interpreted as being driven by a correlation between the size of the X-ray emitting region and black hole mass. A number of studies have also found an anti-correlation between the amplitude of X-ray variability and M_{BH} (e.g. Lu & Yu 2001; Bian & Zhao 2003; Papadakis 2004; Nikolajuk et al. 2004; O’Neill et al. 2005; Gierliński et al. 2008; Zhou et al. 2010). The absence of AGN analogous to the hard state suggests that selection effects may be at work, as all GBHs with accretion rates less than a few per cent of Eddington are hard state objects (e.g., Maccarone 2003), while most AGN surveys have only been able to detect objects radiating at $L/L_{Edd} \gtrsim 0.1$ in large numbers (e.g., Vestergaard 2004; Trump et al. 2009; Kelly et al. 2010).

While studies of AGN variability have many complications, they do have the advantage that the disk and corona emission can be cleanly separated. In contrast, for GBH in the soft state the separation is more difficult as both components emit in X-rays, and the disk component does not exhibit significant variability (e.g., Churazov et al. 2001). Therefore, studies of the disk emission variability are more easily carried out for AGN. Previous studies of AGN optical variability using well-sampled lightcurves have found that the optical variations have dispersions of ~ 10 –20% (Kelly et al. 2009; MacLeod et al. 2010a), with the X-rays varying more on the shorter time scales (e.g., Ulrich et al. 1997; Czerny et al. 2003; Smith & Vaughan 2007; Arévalo et al. 2009), and sometimes also on the longer time scales (Breedt et al. 2010). In addition, the optical PSD can be well described by a power law form $P(f) \propto 1/f^2$ (Givon et al. 1999; Collier & Peterson 2001; Czerny et al. 2003), or, when the lightcurve is long enough, by a Lorentzian centered at zero (Czerny et al. 1999; Kelly et al. 2009; Kozłowski et al. 2010; MacLeod et al. 2010a); i.e., the PSD is $P(f) \propto 1/f^2$, flattening to a constant below some break frequency. Similar to the X-ray PSD, the break frequency of the optical PSD increases with black

hole mass (Collier & Peterson 2001; Kelly et al. 2009; MacLeod et al. 2010a), although not as steeply.

While variability studies of AGN and GBHs have been important for understanding the similarities between these two classes of objects, variability studies are important for other reasons as well. For one, variability is one of the only observational tools available for probing the disk viscosity, as the time scales of variability are expected to depend on viscosity, while the SED is not (Siemiginowska & Czerny 1989; Starling et al. 2004; Frank, King, & Raine 2002). Understanding the disk viscosity is important for understanding the transfer and removal of angular momentum in the disk, which is fundamental to an understanding of the accretion flow. Variability is also a potentially important observational tool for constraining the geometry of the corona, with, for example, studies of quasi-periodic oscillations being consistent with the disk evaporating into a hot inner flow at lower accretion rates (e.g., Cui et al. 1999; Rossi et al. 2004; Done et al. 2007), and the origin of the variability in the QPOs being in the hot corona in the soft state and the disk in the hard state (e.g., Sobolewska & Życki 2006). This is also consistent with the finding of Wilkinson & Uttley (2009) who showed that the disk is responsible for much of the variability in the hard state; however, there is still much work to be done, as it has not been conclusively shown that the source of variability originates in the same region as the emission. In addition, variability may be the most effective observational discriminator between the different accretion states, and thus may provide evidence of radiatively inefficient accretion flows (RIAFs) in AGN, which are believed to be associated with the hard state, should a hard state exist for AGN. A number of RIAF candidates exist (e.g., Ho 1999; Quataert et al. 1999; Trump et al. 2009), but their spectral/timing state is unknown. Studies and confirmation of AGNs in the hard state are particularly important, as the hard state is associated with jet production in GBHs (e.g., Fender 2001; Fender et al. 2004; Körtling et al. 2006), and mechanical feedback from these jets plays an important role in heating intracluster gas and regulating the growth of massive galaxies (Croton et al. 2006; Bower et al. 2006; Sijacki et al. 2007).

Time series exhibiting PSDs of a $1/f$ type are known as ‘long-memory’ processes, and there is an extensive literature on them (e.g., a good reference is Palma 2007). Almost all previous studies of variability in GBHs and AGN have relied on non-parameteric techniques, such as the periodogram or the structure function. However, there are a number of known difficulties in estimating the PSD or structure function non-parameterically (e.g., see Vaughan et al. 2003; Pessah 2007). For one, the empirical estimate of the PSD, known as the periodogram, suffers from windowing effects due to the finite sampling of the lightcurve. These windowing effects include red noise leak and aliasing, which are caused by power leaking into the periodogram from time scales longer and shorter than the maximum and minimum time scales probed by the lightcurve, respectively. Red noise leak and aliasing distort the periodogram, making it potentially difficult to relate the observed periodogram to the true intrinsic PSD. Moreover, irregular sampling further

distorts the periodogram, although this distortion can be alleviated through the use of the Lomb-Scargle periodogram (Lomb 1976; Scargle 1982; Horne & Baliunas 1986; Zechmeister Kürster 2009; Vio et al. 2010). The structure function is not immune to these problems and can similarly be distorted, making its interpretation difficult (Emmanoulopoulos et al. 2010). These distortion problems can be significant for AGN especially, as their observed flux is often much fainter than GBHs and their lightcurves tend to be more irregular and sparsely sampled.

Motivated by these problems, Uttley et al. (2002, see also Done et al. (1992)) developed a powerful Monte Carlo technique for estimating the underlying PSD which accounts for the distorting effects of finite, and possibly irregular, sampling. The basic idea behind the technique is to use Monte Carlo simulations to calculate the expected value of the periodogram as a function of the true underlying PSD, and then to find the true PSD which minimizes a χ^2 goodness of fit measure between the observed periodogram and the expected one. Construction of confidence regions may be obtained through the procedure outlined by Mueller & Madejski (2009). This technique has the advantage that it may be used to fit any arbitrary PSD. However, it also has two disadvantages. First, it is computationally intensive, especially when constructing confidence regions. Second, the χ^2 goodness of fit statistic used to fit the PSDs ignores the covariance in the periodogram among the frequency bins, and is not proportional to the log-likelihood of the periodogram. As such, minimization of the χ^2 statistic of Uttley et al. (2002), while effective, is unlikely to be the most efficient means of constraining the underlying PSD. An alternative Bayesian approach based on an approximation to the likelihood function of the periodogram has been developed by Vaughan (2010). An additional likelihood-based approach has been developed by Miller et al. (2010) with the difference being that the likelihood function is calculated in the time domain. Unfortunately these two alternative approaches do not completely incorporate the distortion in the PSD due to finite sampling of the lightcurve, such as that caused by red noise leak, although in principle the PSD model used by Miller et al. (2010) can be modified to correct for this. Indeed, it is very difficult to derive an analytic expression for the likelihood function of the periodogram for a finite and irregularly sampled lightcurve, and in many cases may be impossible.

An alternative and complementary approach to Fourier-based techniques is to model the lightcurve as a parameterized stochastic process, with the parameters of the model being related to the underlying PSD (or rather, the PSD being a function of the parameters of the process). Under this approach, the parameters of the model are estimated directly from the lightcurve itself; no Fourier transforms are performed, and thus there is no spectral distortion. Moreover, modeling the lightcurve in the time domain potentially can provide further insight on features in the power spectrum, such as break frequencies, as it is not always apparent how to interpret the PSD. Time-domain modeling was advocated for by Kelly et al. (2009, hereafter KBS09, see also Scargle (1981) and Rybicki & Press (1992)) within the context of estimating the characteristic time scale of AGN optical

variability (or equivalently, the break frequency of the optical PSD), and they developed a Bayesian approach for estimating the parameters. KBS09 modeled AGN optical lightcurves as Gaussian Ornstein-Uhlenbeck (OU) process, the power spectrum of which is a Lorentzian centered at zero, and showed that this process is consistent with the optical lightcurves of AGN for their sample. Subsequent work has confirmed that the OU process provides a good description of AGN optical variability, at least on time scales between a few days and several years (Kozłowski et al. 2010; MacLeod et al. 2010a), and of blazar sub-mm variability (Strom et al. 2010). Moreover, the OU process provides a framework in which to measure the time lags between the AGN broad line region and optical continuum (Zu et al. 2010) and select quasars (Kozłowski et al. 2010; Butler & Bloom 2010; MacLeod et al. 2010b).

In this work we extend the method of KBS09 to enable more flexible modeling of the PSD of accreting black hole systems. We model the lightcurves as a linear expansion of OU processes, which enable us to approximate many of the features seen in the PSDs of GBHs and AGN, particularly the bending power-law forms. We derive the likelihood function for this statistical model and perform statistical inference within a Bayesian framework, thus enabling one to calculate the probability distribution of the parameters, such as the break frequencies, given the data. Because our method is based on the likelihood function, it uses all of the information in the data. Furthermore, it fully accounts for measurement errors, irregularly sampling, red noise leak, and aliasing. Fitting is performed on the entire lightcurve simultaneously regardless of the sampling, thus enabling one to easily combine lightcurves obtained from different instruments and sampling time scales. These properties make our technique particularly attractive for obtaining constraints on PSD features for poorly sampled lightcurves of faint objects, as our Bayesian method uses all of the information in the data. Calculation of the likelihood function is computationally efficient, and we are able to calculate a maximum-likelihood estimate of the PSD in under a minute¹. The primary disadvantage of our method is that, while flexible, it cannot fit arbitrary PSDs; for this, one should use the method of Uttley et al. (2002), or a combination of the two techniques.

While the OU process, and similarly the mixture of OU processes, is useful for fitting PSDs, and thus quantifying variability, it is not always clear how to interpret the best-fit OU process astrophysically, or the PSD in general. Titarchuk et al. (2007) studied the linear diffusion equation for an accretion disk with a driving noise term as a model for the PSDs of accreting black holes, showing that features in the PSD depend on the viscosity of the accretion flow. In this work we will show how the mixture of OU processes arises as the solution to the linear diffusion equation, perturbed by a random spatially-correlated white noise field. This interpretation of the mixed OU process may be considered to be among the ‘perturbation’ class of astrophysical models for variability of GBHs and AGN, with the variability arising from

¹ The calculation was done on a lightcurve with ~ 3000 data points in IDL on a Mac Pro with two 3.2 GHz Quad-Core Intel Xeon processors

small random accretion rate perturbations that propagate inwards through the accretion flow, making the observed variations the product of perturbations that occur at larger radii (e.g., Lyubarskii 1997; King et al. 2004; Arévalo & Uttley 2006; Janiuk & Czerny 2007; Titarchuk et al. 2007). The perturbation class of models for variability also explains the correlation between flux and absolute RMS variability seen in both GBHs and AGN (e.g. Uttley & McHardy 2001), which Uttley et al. (2005) show is very well approximated as being due to a Gaussian process on the logarithmic scale.

Finally, we note that the perturbation class of models for variability is only applicable to the broad-band flickering noise seen in GBH and AGN lightcurves, and we do not address the more catastrophic, and seemingly not stochastic, changes that have been observed in the lightcurves of GRS 1915+105 (e.g., Belloni et al. 2000). These may occur due to accretion disk instabilities, such as radiation pressure instabilities (e.g., Shakura & Sunyaev 1976; Lightman & Eardley 1974; Czerny et al. 2009), or the thermal-viscous ionization instability (Lin & Shields 1986; Siemiginowska et al. 1996; Janiuk et al. 2004). Furthermore, we stress that the astrophysical interpretation of the mixed OU process as a model for the fluctuations from GBHs and AGN is based on the linear diffusion equation, which is surely an oversimplification, and MHD simulations must be performed for studying more physically motivated models for variability of accreting black holes, as done by, e.g., Armitage & Reynolds (2003), Schnittman et al. (2006), Moscibrodzka et al. (2007), Reynolds & Miller (2009), and Noble & Krolik (2009). Rather, we study the mixed OU process as a solution to the stochastic linear diffusion equation in order to provide a guide for interpreting the best-fit model and PSD features of lightcurves, both real and simulated, as analytical solutions may be obtained.

The format of the paper is as follows: In § 2 we describe the mixed OU process statistical model for the lightcurves of GBHs and AGN. In § 3 we show that the mixed OU process is generically the solution to the linear diffusion equation. In § 4.1 we derive the likelihood function of the mixed OU process parameters, and posterior probability distribution of the parameters given an observed lightcurve. In § 5 we apply the mixed OU process to an X-ray lightcurve of Cygnus X-1 in the low/hard state, the X-ray lightcurves of 10 local well-studied AGN, and the optical lightcurves of a sample of AGN. Finally, in § 6 we summarize our results.

2. THE STATISTICAL MODEL

2.1. The Ornstein-Uhlenbeck Processes

In this section we give a brief overview of the properties of the OU process that are relevant for our work. Further details can be found in Kelly et al. (2009, see also Gillespie (1996) and Gardiner (2004)), who refer to this process as a first-order continuous autoregressive process. The OU process, $X(t)$, is a simple stochastic process by which the quantity of interest (say, the logarithm of the luminosity or accretion rate) responds to an input noise process with an exponential decay to its mean. Mathematically, the OU process is defined by the following stochastic differential equation:

$$dX(t) = -\omega_0(X(t) - \mu)dt + \varsigma dW(t), \quad \omega_0, \varsigma > 0. \quad (1)$$

The parameters of the process are the characteristic frequency, ω_0 , the mean value of the process, μ , and the amplitude of the driving noise process, ς . The term ς^2 has units of $\text{RMS}^2 \text{ sec}^{-1}$, and thus ς gives the rate at which variability power is injected into the stochastic process $X(t)$. The term $W(t)$ denotes a Wiener process (i.e., a Brownian motion), and its derivative is white noise. Although in this work we will focus on the special case when $W(t)$ is a Wiener process, the results outlined here for the OU process, such as the form of its PSD, are valid for a more general class of stochastic processes called Lévy processes. For completeness, we give a brief description of Lévy processes in the appendix. It is apparent from setting $\varsigma = 0$ in Equation (1) that $X(t)$ decays to its mean value with an e -folding time scale of $\tau = 1/\omega_0$. The time scale τ is often called the relaxation time scale of the process; in this work we will refer to τ as the characteristic time scale of the process, as τ is related to the break frequency in the power spectrum of $X(t)$.

When the driving noise, $dW(t)$, is white, the OU process is stationary and Markov. A stationary process is one whose joint probability distribution does not change when shifted in time, and a Markov process is one whose future states only depends on the current state. In addition, if $W(t)$ has zero mean and unit variance the autocovariance function of the OU process is

$$R_{OU}(t) = \frac{\varsigma^2 \tau}{2} e^{-|t|/\tau}. \quad (2)$$

It follows from setting $t = 0$ in Equation (2) that the variance of the OU process is $\varsigma^2 \tau / 2$, and that the autocorrelation function has an exponential decay with $\tau = 1/\omega_0$ being the decorrelation time scale. The power spectrum of the OU process is given by the Fourier transform of the autocovariance function:

$$\begin{aligned} P_{OU}(\omega) &= \frac{1}{2\pi} \int_{-\infty}^{\infty} e^{-i\omega t} R_{OU}(t) dt \\ &= \frac{\varsigma^2}{2\pi} \frac{1}{\omega_0^2 + \omega^2}. \end{aligned} \quad (3)$$

The power spectrum of an OU process is flat for frequencies $\omega \ll \omega_0$, and decays as $1/\omega^2$ for frequencies $\omega \gg \omega_0$. Hence the association of τ as a characteristic time scale of the process: the OU process, $X(t)$, resembles white noise on time scales long compared to τ , and resembles red noise on time scales short compared to τ . Note that if one calculates the power spectrum in terms of ordinary frequencies instead of angular frequencies, then $\tau = 1/(2\pi f_0)$, where $f_0 = \omega_0/(2\pi)$. This implies that simply fitting the break in the power spectrum as a function of ordinary frequency f will overestimate τ by a factor of 2π .

2.2. Mixtures of Ornstein-Uhlenbeck Processes

We can build on the OU process to develop more flexible models that enable modeling of more complex power spectra. In this work we consider a mixture of OU processes with independent driving noises for constructing a process with a power spectrum of the form exhibited by the X-ray lightcurves of GBH and AGN. We define a

discrete mixture of OU processes as

$$Y_M(t) = \mu + \sum_{i=1}^M c_i X_i(t). \quad (4)$$

Here, c_1, \dots, c_M is a set of mixing weights, and $X_1(t), \dots, X_M(t)$ is a set of OU processes with characteristic frequencies $\omega_1, \dots, \omega_M$ and driving noise amplitudes $\varsigma_1, \dots, \varsigma_M$. A continuous version of Equation (4) is described in the Appendix, although we do not use it in this work. The autocovariance function of $Y_M(t)$ is

$$R_{Y,M}(t) = \sum_{i=1}^M \frac{c_i^2 \varsigma_i^2 \tau_i}{2} e^{-|t|/\tau_i}, \quad (5)$$

where we have used the fact that $\tau_i = 1/\omega_i$. The sum of exponentials in Equation (5) falls off more slowly than a single exponential function, and therefore the autocorrelation function of the mixed OU process falls off more slowly than the autocorrelation function of the individual OU processes. In other words, the mixed OU process exhibits longer range dependency than a single OU process, and therefore is better suited for modeling lightcurves with long time scale dependencies.

The power spectrum of $Y_M(t)$ is

$$P_{Y,M}(t) = \sum_{i=1}^M \frac{c_i^2 \varsigma_i^2}{2\pi} \frac{1}{\omega_i^2 + \omega^2}. \quad (6)$$

From Equations (5) and (6) it is apparent that the contribution of an individual OU process to the variability amplitude of a lightcurve depends on the product $c_i \varsigma_i$, and thus the two parameters are degenerate. Therefore, for simplicity in this work we only consider the case where all of the individual OU processes have the same value of ς .

In Figure 1 we plot a mixed OU process sampled at the three different time intervals. The mixing weights for this example were chosen such that the power spectrum of the simulated lightcurve was flat below a low-frequency break, ω_L , decays as $1/f$ above the low-frequency break, and then steepened to $1/f^2$ above a high-frequency break, ω_H , similar to what is seen in the X-ray lightcurves of accreting black hole systems. Thus, the simulated lightcurves probe the ‘white’ noise, ‘pink’ noise, and ‘red’ noise regions of the PSD. We constructed these lightcurves assuming that the logarithm of the flux follows a mixed OU process with $\mu = 0, \varsigma = 1, \tau_H = 0.1 = 1/\omega_H$, and $\tau_L = 10 = 1/\omega_L$, and that the driving noise is Gaussian white noise. In general, we model the logarithm of the flux as a Gaussian mixed-OU process, as this is consistent with the flux-rms correlation seen in the X-ray variations of GBHs and AGN (Uttley & McHardy 2001) and the log-normal distribution of fluxes for Cygnus X-1 (Uttley et al. 2005). In addition, the same seed for the random number simulator was used in order enable a more direct comparison between the lightcurves. As is apparent, the mixed OU process can appear very different depending on which time scales are probed by the observation.

Equation (B7) in the Appendix demonstrates that the power spectrum of the continuous mixed OU process, with mixing function given by Equation (B2), exhibits

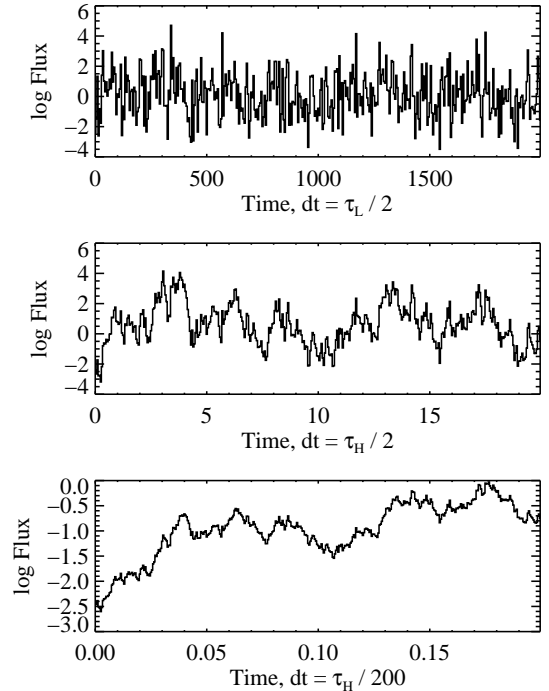


Figure 1. Simulated lightcurves illustrating the mixed OU process. The lightcurves were generated using $\mu = 0, \varsigma = 1, \tau_H = 0.1, \tau_L = 10$, independent Gaussian white driving noises, and a common random number generator seed. The three lightcurves probe the white noise (flat) part of the power spectrum (top), the ‘pink’ noise ($1/f$) part of the power spectrum (middle), and the red noise ($1/f^2$) part of the power spectrum. The mixed OU process can look very different depending on the time scales probed by the observations.

the same behavior that is seen in the power spectrum of the X-ray lightcurves of GBHs and AGN. This therefore suggests that the mixed OU process well represents the fluctuations in the X-ray lightcurves of GBH and AGN, and may hold clues to the physical origin of the X-ray fluctuations. Moreover, we have identified a process which gives an explicit connection between the break frequencies in the X-ray power spectra and characteristic time scales. This is important, because it is not always apparent how to connect a feature in the power spectrum with behavior in the time-domain. For example, we note that the characteristic time scales correspond to break frequencies when calculating the power spectrum in terms of ω , but simply taking the inverse of the ordinary frequency, $1/f$, corresponding to the break will overestimate τ_L and τ_H by a factor of 2π .

Physically, a mixed OU process may represent the X-ray fluctuations of GBH and AGN under the propagating disturbance model, originally developed by Lyubarskii (1997). In this model, stochastic disturbances originate in the region of the accretion disk outside of the X-ray emitting region. These disturbances propagate inwards and modulate the X-ray emitting region, which cause fluctuations in the X-ray flux. Because many physically relevant time scales increase with radius, the X-ray flux varies on a broad range of time scales due to the disturbances originating over a broad range in radii. If the disturbances at various radii are independent and are well described by an OU process with characteris-

tic time scales that increase with radius, then the X-ray flux should be well described by a mixture of OU processes. The fact that we can construct a mixed OU process with PSD similar to the X-ray power spectra of GBH and AGN is consistent with this interpretation. In this case, the break frequencies correspond to the characteristic time scales of the disturbances at the maximum and minimum radii of the region that contributes to modulating the X-ray emission. We develop this interpretation further in § 3.

3. MIXED OU PROCESS AS RESULTING FROM STOCHASTIC DIFFUSION IN THE ACCRETION DISK

Similar to us, many authors have attempted to identify a particular stochastic process for the accretion rate perturbations. While we model the accretion rate perturbations as following an OU process, Arévalo & Uttley (2006), Titarchuk et al. (2007), and Misra & Zdziarski (2008) have shown that a power spectrum with a $1/f$ region can also be created when the accretion rate perturbations have a Lorentzian power spectrum, i.e., when the disturbances are quasi-periodic. Perturbations of this sort are expected if, for example, the perturbations are due to Rayleigh-Taylor instability (Titarchuk et al. 2007). King et al. (2004, see also Mayer & Pringle (2006) and Janiuk & Czerny (2007)) model the fluctuations as resulting from a magnetic field modeled as a first order autoregressive process, which is a discrete form of the OU process (e.g., Brockwell & Davis 2002). We can build on the work of Wood et al. (2001) and Titarchuk et al. (2007) to show that a mixed OU process can model the viscous response of the accretion disk subject to a stochastic driving noise field, for the special case when the diffusion equation is linear.

Conservation of mass and angular momentum result in material in the disk obeying a nonlinear diffusion equation:

$$\frac{\partial \Sigma}{\partial t} = \frac{3}{r} \frac{\partial}{\partial r} \left[r^{1/2} \frac{\partial}{\partial r} (r^{1/2} \nu \Sigma) \right]. \quad (7)$$

Here, Σ is the surface density of the disk and ν is the kinematic viscosity. Under the assumption that the rotational frequency of the disk is equal to the Keplerian value, the accretion rate is given by (Wood et al. 2001)

$$\dot{M}(r, t) = 6\pi r^{1/2} \frac{\partial}{\partial r} (r^{1/2} \nu \Sigma). \quad (8)$$

We can use Equations (7) and (8) to study the evolution of accretion rate perturbations about the average steady state solution. Following Wood et al. (2001) and Titarchuk et al. (2007), define $x = r^{1/2}$ and a perturbation to the quantity $r^{1/2} \nu \Sigma$ as $u(x, t) = x \Delta(\nu \Sigma)$, and therefore $\Delta \dot{M}(r, t) \propto \partial u(x, t) / \partial x$. The nonlinear diffusion equation for a single perturbation can now be written as (e.g., Frank, King, & Raine 2002)

$$\frac{\partial u}{\partial t} = \frac{3}{4} \frac{\partial u}{\partial \Sigma} \frac{\partial^2 u}{\partial x^2}. \quad (9)$$

When ν is independent of Σ , Equation (9) becomes a linear diffusion equation.

Equation (9) only describes the evolution of a single perturbation, but in order to create flickering in $u(x, t)$

we need to introduce a persistent source of the fluctuations. We can introduce fluctuations to $u(x, t)$, and therefore to $\Delta \dot{M}(r, t)$, by introducing a stochastic source term to Equation (9). For simplicity, we only study the linear form of Equation (9), and therefore assume that the viscosity is independent of surface density. While it is unlikely that the viscosity is independent of Σ , it is still illuminating to study the linear form of the diffusion equation in order to better understand how the disk responds to a stochastic driving noise, as it permits an analytical treatment. Denote the stochastic source as $\partial W(x, t) / \partial t$, where $\partial W(x, t) / \partial t$ is a spatially dependent white noise², and therefore $W(x, t)$ is a Wiener random field. By definition, $\partial W(x, t) / \partial t$ has a flat power spectrum and zero mean. The mean of $W(x, t)$ is also zero, and the covariance of $W(x, t)$ is

$$E[W(x, t)W(y, s)] = \zeta(x, y) \min(t, s), \quad (10)$$

where $E(x)$ denotes the expected value of x , and $\zeta(x, y)$ defines the spatial covariance of the Wiener random field. The Wiener process is essentially a continuous time Brownian motion, and therefore the Wiener random field $W(x, t)$ may be viewed as an infinite set of Brownian motions indexed by the parameter x . If there are no spatial correlations for $W(x, t)$, then $\zeta(x, y) = \delta(x - y)$ and $\partial W(x, t) / \partial t$ is called a ‘space-time’ white noise; however, in this case, solutions to the linear stochastic diffusion equation only exist for the case of one spatial dimension (Chow 2007).

We assume that the perturbations to the accretion rate only exist in a bounded accretion flow defined over a region $0 < x < x_{max}$, where x_{max} represents the outer edge of the flow. We adopt the boundary condition given by Wood et al. (2001) and Titarchuk et al. (2007), with $u(0, t) = 0$ and $\partial u(x_{max}, t) / \partial t = 0$. The first boundary condition assures that the perturbations of Σ go to zero at the inner boundary of the disk, and the second ensures the the disk accretes the perturbations, i.e., the perturbations can only leave through the inner boundary. Including a stochastic source in the linear diffusion equation, our stochastic model for the accretion rate perturbations is defined by the following set of Equations:

$$\frac{\partial u(x, t)}{\partial t} = \frac{3\nu(x)}{4} \frac{\partial^2 u(x, t)}{\partial x^2} + \frac{\partial W(x, t)}{\partial t} \quad (11)$$

$$\Delta \dot{M}(x, t) = 3\pi \frac{\partial u(x, t)}{\partial x} \quad (12)$$

$$u(x, 0) = u_0(x) \quad (13)$$

$$u(0, t) = 0 = \frac{\partial u(x_{max}, t)}{\partial t}. \quad (14)$$

Equations (11)–(14) can be solved using standard methods developed for stochastic partial differential equations, and a good introduction is Chow (2007).

Before presenting the solution, a couple of remarks are warranted. First, the model defined by Equations (11)–(14) is clearly only an approximation for several reasons.

² This notation should not be strictly interpreted as a traditional derivative, as the definitions and rules used in stochastic calculus are not necessarily the same as those of ordinary calculus. However, we ignore this mathematical technicality, as the notation $\partial W(x, t) / \partial t$ conveys the appropriate interpretation of $W(x, t)$ as the integral of $\partial W(x, t) / \partial t$ over t .

As mentioned before, the actual viscous response of the disk will be nonlinear, as the viscosity also likely depends on the surface density. In addition, for the noise process assumed above, there is nothing to prevent the linear model from producing negative values of Σ and \dot{M} , which are unphysical. A better approach would be to postulate a stochastic model for the viscosity which ensures positivity of the solution, and then solve Equation (9) numerically using this prescription for $\nu(r, \Sigma, t)$. However, in this work our goal is to study the simpler model, for which analytical solutions are possible, in order to better understand how the disk responds to a random driving noise field, and thus provide some insight on how to connect features in the power spectra to the physics of the accretion disk. Moreover, we will show that the solution to the linear diffusion equation is a mixture of OU-processes, providing justification for their use in modeling variability. Second, it is important to note that the stochastic noise field in the partial differential equation, $\partial W(x, t)/\partial t$, is the time derivative of the process which is the source of the random perturbations, and is not the process itself. And third, the physical interpretation of the noise process is left unspecified, however, as many authors have suggested, $\partial W(x, t)/\partial t$ may represent fluctuations in $\partial u(x, t)/\partial t$ which are the result of turbulent and chaotic MHD effects (e.g., Lyubarskii 1997; King et al. 2004). Indeed, MHD turbulence has been observed in numerical simulations (e.g., Hawley & Krolik 2001).

The solution to Equations (11)–(14) can be expressed through the eigenfunctions of the diffusion operator. The eigenfunctions, $e_k(x)$, and eigenvalues, ω_k , are defined by

$$\frac{3\nu(x)}{4x^2} \frac{d^2}{dx^2} e_k(x) = \omega_k e_k(x), \quad (15)$$

subject to the appropriate boundary conditions. Eigenfunctions and eigenvalues are given in Wood et al. (2001) and Titarchuk et al. (2007), respectively, for the case where the viscosity $\nu(x)$ is a power-law in x . The eigenfunctions are orthonormal with respect to the weighting function $p(x) = 4x^2/(3\nu(x))$, and form a complete set. The solution to Equations (11)–(14) is then given by Chow (2007)

$$u(x, t) = \sum_{k=1}^{\infty} u_k(t) e_k(x), \quad (16)$$

where $u_k(t)$ are a set of stochastic processes. In order to determine $u_k(t)$, we first note that if the spatial covariance function of the driving noise, $\varsigma(x, y)$, exists in the space spanned by the eigenfunctions, then we can express it as an eigenfunction expansion,

$$\varsigma(x, y) = \sum_{k=1}^{\infty} \varsigma_k^2 e_k(x) e_k(y), \quad (17)$$

where the coefficients are

$$\varsigma_k^2 = \int_0^{x_{max}} \int_0^{x_{max}} \varsigma(x, y) p(x) e_k(x) p(y) e_k(y) dx dy. \quad (18)$$

The random field $W(x, t)$ can then be expressed as (e.g.,

Chow 2007)

$$W(x, t) = \sum_{k=1}^{\infty} \varsigma_k e_k(x) w_k(t), \quad (19)$$

where $\{w_k(t)\}$ are a sequence of independent and identically distributed Brownian motions.

Inserting Equations (15), (16), and (19) into Equations (11) and (13) produces an infinite set of ordinary stochastic differential equations:

$$du_k(t) = -\omega_k u_k(t) dt + \varsigma_k dw_k(t), \quad k = 1, 2, \dots, \quad (20)$$

$$u_k(0) = \int_0^{x_{max}} u_0(x) p(x) e_k(x) dx. \quad (21)$$

Comparison of Equations (20) and (21) with Equation (1) shows that $u_k(t)$ are a set of independent OU processes with initial condition $u_k(0)$. Therefore, the solution to the linear diffusion equation defined by Equations (11)–(14) is

$$u(x, t) = \sum_{k=1}^{\infty} [u_k(0) e_k(x) e^{-\omega_k t} + \varsigma_k e_k(x) X_{ou}(t, \omega_k)] \quad (22)$$

$$\Delta \dot{M}(x, t) \propto \sum_{k=1}^{\infty} \left[u_k(0) \frac{\partial e_k(x)}{\partial x} e^{-\omega_k t} + \varsigma_k \frac{\partial e_k(x)}{\partial x} X_{ou}(t, \omega_k) \right] \quad (23)$$

where $X_{ou}(t, \omega_k)$ is an OU process defined by Equation (1) with white driving noise, $\mu = 0$, and $\varsigma = 1$. The first eigenvalue is roughly given by the viscous timescale at the outer edge of the disk, τ_{visc} , depending on how $\nu(x)$ depends on x . In particular, if $\nu(x)$ has a power-law dependency on x , then $\omega_1 \propto 1/\tau_{\text{visc}}$ (Titarchuk et al. 2007). In addition, if the driving noise field is a Gaussian process, then the accretion rate perturbations will also be a Gaussian process.

In general, we are interested in the stationary solution, which occurs when $t \rightarrow \infty$. As a practical matter, this occurs after a few viscous times have passed. In this case, the initial condition has been forgotten, and the solution to the linear stochastic diffusion equation is a mixture of OU processes, with the characteristic frequencies given by the eigenvalues of the linear diffusion operator, the mixing weights given by the product of the eigenfunctions of the linear diffusion operator and the coefficients of the eigenfunction expansion of the spatial covariance of the driving noise field. Then, the covariance function of the accretion rate perturbations is

$$\text{Cov}(\Delta \dot{M}(x, t), \Delta \dot{M}(y, s)) = \sum_{k=1}^{k=\infty} \frac{\varsigma_k^2}{2\omega_k} \frac{\partial e_k(x)}{\partial x} \frac{\partial e_k(y)}{\partial y} e^{-\omega_k |t-s|}, \quad (24)$$

and the power spectral density for fluctuations as a function of radius is

$$P_{\Delta \dot{M}}(x, \omega) = \sum_{k=1}^{\infty} \frac{\varsigma_k^2}{2\pi} \left(\frac{\partial e_k(x)}{\partial x} \right)^2 \frac{1}{\omega_k^2 + \omega^2}. \quad (25)$$

The X-ray emission of accreting black holes is thought to be released in the inner regions of the disk, and therefore the behavior of the accretion rate fluctuations at small x is of primary interest. It is illuminating to investigate asymptotic behavior of the power spectrum at

$x \rightarrow 0$ for the case where $\nu(x) \propto x^\alpha$. As per the discussion in § 2.2, the power spectrum of a mixed OU process is flat on frequencies shorter than ω_1 , and therefore the fluctuations are decorrelated on time scales longer than the viscous time scale at x_{max} . However, on time scales short compared to the viscous time scale, the situation is more complicated as the power spectrum also depends on the spatial covariance structure of the driving noise field, $\zeta(x, y)$, through the set of ζ_k . For simplicity, we first assume that there is no spatial correlation in the driving noises, and therefore $\zeta(x, y) = \delta(x - y)$ and $\zeta_k = 1$ for all k . Following Titarchuk et al. (2007), one can then show that the power spectrum of the accretion rate perturbations at small radii decays as a power-law on timescales short compared to the viscous time scale, with the slope of the power-law decay steepening when the viscosity increases less steeply toward larger radii. Therefore, if the viscosity increases more steeply toward higher radii, then at small radii the longer time scale perturbations are more suppressed relative to the short time scale perturbations.

In order to investigate the effect that the spatial correlations in the noise field have on the observed power spectra of $\Delta\dot{M}(x = 0, t)$, we study the case of $\nu(x) \propto x^2$. In this case the eigenfunctions are sin functions and the eigenvalues are $\omega_k \propto (2k - 1)^2$ (e.g., Wood et al. 2001). One can show that the power spectrum for $\Delta\dot{M}$ at small radii is then

$$P_{\Delta\dot{M}}(x, \omega) \propto \sum_{k=1}^{\infty} \frac{\zeta_k^2 \omega_k}{\omega_k^2 + \omega^2} \quad (26)$$

$$\omega_k = (2k - 1)^2 \frac{\pi}{2}. \quad (27)$$

As an example, suppose that the spatial correlations for $W(x, t)$ decay exponentially in radius with some characteristic radius r_0 :

$$\zeta(x, y) \propto e^{-|x^2 - y^2|/r_0}. \quad (28)$$

Then, in this case, the coefficients in the eigenfunction expansion, ζ_k^2 , are constant for $\omega_k \ll r_0/r_{max}$ and fall off as $\zeta_k^2 \propto 1/\omega_k^2$ for $\omega_k \gg r_0/r_{max}$. Inserting this form for ζ_k^2 into the Equation for the power spectrum of $\Delta\dot{M}(0, t)$ suppresses the higher frequency modes in the eigenfunction expansion, thus suppressing the fluctuations on short time scales. In particular, for a power spectrum of the form Equation (26), a second break will appear near $\omega_{r_0} \sim 1/\tau_{r_0}$, producing a second region which decays even faster than the intermediate region. The second characteristic time scale, τ_{r_0} , corresponds to the time it takes a perturbation traveling at the viscous speed, $v_r \sim r_{max}/\tau_{visc}$, to travel across a region corresponding to the spatial scale of the driving noise field:

$$\tau_{r_0} \sim \frac{r_0}{v_r} \sim \frac{r_0}{r_{max}} \tau_{visc} \quad (29)$$

This may be the source of the high frequency break seen in X-ray power spectra of GBH and AGN, although it may also be due to an abrupt change in the accretion geometry or viscosity (Churazov et al. 2001; Psaltis & Norman 2000). Furthermore, we note that if the amplitude of the driving noise field increases with radius, then ζ_k will decrease with increasing k , steepening

the slopes in both the intermediate region ($\omega_1 \lesssim \omega \lesssim \omega_{r_0}$) and the high-frequency region $\omega \gtrsim \omega_{r_0}$. However, a decrease in viscosity with increasing radius also has this effect, and thus the two situations are degenerate.

Finally, we note that in order to connect the power-spectrum of luminosity fluctuations with that of accretion rate fluctuations, heat and photon diffusion effects must also be considered. The diffusion of heat and photons are both governed by diffusion equations, and the radiative output of the disk may be described as resulting from the convolution of the solution to the heat and photon diffusion equations with the accretion rate fluctuations (e.g., Titarchuk et al. 2007), which are stochastic. The power spectrum of the radiative output is then the product of the power spectra for the accretion rate perturbations and the power spectra for the solution to the heat and photon diffusion equations. While a detailed treatment of the effects of heat and photon diffusion is beyond the scope of this work (but see Sunyaev & Titarchuk 1980, 1985; Titarchuk et al. 2007), we note that based on the above discussion and the results of Titarchuk et al. (2007), the power spectra of the solution to the linear heat and photon diffusion equations will also be of the form of Equation (6). Therefore, additional breaks will occur at frequencies corresponding to the characteristic frequencies of the heat and photon diffusion equations, and the power spectra of the radiative output will steepen even further above these breaks. Thus, the observed fluctuations in the emission from accreting black holes may be interpreted as the result of the response of the disk to a random noise field, where the viscous, thermal, and radiative response of the disk act as a series of low-pass filters on the driving noise field, sequentially suppressing the variability on time scales short compared to the characteristic time scales for viscous, thermal, and photon diffusion. Furthermore, if the noise field is spatially correlated, then variability on time scales short compared to the drift time scale for the characteristic length of the spatial correlations is also suppressed. Thus, breaks are expected to exist in the power spectra at the frequencies corresponding to these time scales, and the slope of the power spectra in the different regions contains information on the viscous, thermal, and radiative structure of the accretion flow, as well as the structure of the driving noise field.

For completeness, we summarize here the some of the results from the above discussion:

- The mixed OU process is the solution to the linear diffusion equation, subject to a random driving noise field. The mixing weights are the product of the eigenfunctions of the linear diffusion operator and the coefficients of the eigenfunction expansion of the covariance function of the driving noise field. The characteristic frequencies of the OU processes are the eigenvalues of the linear diffusion operator, subject to the appropriate boundary conditions.
- The power spectrum of accretion rate perturbations at small radii, where most of the energy is thought to be released, is flat on time scales longer than the viscous time scale at the largest radii. On timescales shorter than τ_{visc} , the power spectrum has the form $C_1/\omega^2 < P_{\Delta\dot{M}}(\omega) < C_2$, where C_1 and C_2 are constants.

- There is a second break in the power spectrum of $\Delta\dot{M}$ on time scales short compared to the crossing time of a perturbation traveling at the viscous speed across a region of length similar to the characteristic spatial correlation length of the driving noise field. The power spectrum of $\Delta\dot{M}$ steepens on frequencies higher than this break.
- If the viscosity of the disk increases toward higher radii, then in the inner region of the disk the long time scale fluctuations are suppressed compared to the short time scale fluctuations, thus flattening the power spectrum. Similarly, if the amplitude of the driving noise increases toward smaller radii, the power spectrum also flattens. Thus, these two effects are degenerate and cannot be distinguished on the basis of power spectra alone.
- Heat and photon diffusion can introduce additional breaks in the power spectra of the emission from accreting black holes, with the power spectra steepening above these breaks.

4. FITTING THE MIXED OU PROCESS

In the previous section we have suggested an interpretation of the mixed OU process developed in this work in terms of the viscous response of the accretion disk subject to a random driving noise field. However, the mixed OU process is not limited to linear diffusion models for viscous evolution of the accretion disk, and in fact one can go through the same steps outlined above to show that the mixed OU process is a solution for many parabolic stochastic partial differential equations, and thus will also describe, say, the diffusion of heat in the disk, which is governed by the heat equation. However, regardless of the physical mechanism, the mixed OU process provides an accurate statistical description of the lightcurves of GBH and AGN, in the sense that it reproduces much of the shape of the power spectra of these objects. As a result, estimation of the break frequencies can be done directly from the observed lightcurve, and is therefore free of the biases due to windowing effects, which are inherent in fitting of power spectra. Some features are not captured by this process, such as quasi-periodic oscillations and nonlinear effects. An additional quasi-periodic component can be modeled as a solution to a set of hyperbolic stochastic partial differential equations, in particular the random wave equation. However, inclusion of quasi-periodic oscillations to our model is beyond the scope of this work.

4.1. The Likelihood Function

The mixed OU process may be fit using maximum-likelihood or Bayesian techniques. This has the advantage that the parameters for the process are estimated directly from the observed lightcurve utilizing all of the information in the data. In particular, the estimates of the parameters for the power spectrum model are not biased by measurement errors, irregular sampling, or other windowing effects due to the finite time span of the lightcurve, such as red noise leak. While these biases may be corrected for using Monte Carlo methods (Uttley et al. 2002), such methods are also computationally intensive and rely on a χ^2 statistic. Indeed, these

benefits of time domain modeling are our primary motivation in developing the mixed OU process model; we sought to obtain a means of estimating the break frequencies and variability amplitude of X-ray lightcurves in a manner that was free of the biases that can affect frequency domain techniques.

In order to calculate the likelihood function of the lightcurve, it is necessary to assume a probability distribution for the driving noise process. In this work we assume that the driving noise $dW(t)$ is Gaussian white noise (i.e., $W(t)$ is the Gaussian Wiener process). In the context of the linear diffusion equation interpretation, this is equivalent to assuming that the driving noise field is a Gaussian process. Denote the n observed flux values as y_1, \dots, y_N , sampled at time values of t_1, \dots, t_N . The observed flux values have independent Gaussian measurement errors with variances v_1, \dots, v_N . We denote $\mathbf{y}, \mathbf{t}, \mathbf{v}$ to be the vectors containing the N values of flux, time, and measurement error variance. In this case it is straightforward to calculate the likelihood function, as the lightcurves follow a N -dimensional multivariate normal distribution with mean μ and covariance matrix $R_Y(\mathbf{t}) + \text{diag}(\mathbf{v})$, where $R_Y(\mathbf{t})$ is given by Equation (5) calculated at the appropriate values, and $\text{diag}(\mathbf{v})$ operates on the vector \mathbf{v} by constructing a diagonal matrix with \mathbf{v} along the diagonal.

Unfortunately, direct calculation of the likelihood becomes computationally prohibitive for most reasonable values of N . However, for the discrete mixture the likelihood for an observed lightcurve, modeled according to Equation (4), can be efficiently calculated by obtaining a state-space representation of the lightcurve, and then using the Kalman recursions¹. Using these techniques, the likelihood function, $p(\mathbf{y}|\mathbf{c}, \omega, \mu, \hat{\varsigma})$, is calculated using the following recursion formulae:

$$p(\mathbf{y}|\mathbf{c}, \omega, \mu, \hat{\varsigma}) = \prod_{i=1}^n [2\pi\Delta_i]^{-1/2} \exp\left\{-\frac{1}{2}\frac{(\hat{y}_i - y_i)^2}{\Delta_i}\right\} \quad (30)$$

$$\hat{y}_1 = \mu \quad (31)$$

$$\Delta_1 = \frac{\varsigma^2}{2} \sum_{j=1}^M c_j^2 \tau_j \quad (32)$$

$$\hat{\mathbf{x}}_1 = \mathbf{0} \quad (33)$$

$$\mathbf{\Omega}_1 = \text{diag}\left(\frac{\varsigma^2}{2} \left[\frac{c_1}{\omega_1}, \dots, \frac{c_M}{\omega_M}\right]^T\right) \quad (34)$$

$$\mathbf{A}_i = \text{diag}\left(\exp\{-(t_i - t_{i-1})[\omega_1, \dots, \omega_M]^T\}\right) \quad (35)$$

$$\mathbf{\Theta}_i = \mathbf{A}_i \mathbf{\Omega}_i \mathbf{c} \quad (36)$$

$$\hat{\mathbf{x}}_i = \mathbf{A}_i \hat{\mathbf{x}}_{i-1} + \frac{\mathbf{\Theta}_i}{\Delta_{i-1}} (y_{i-1} - \mu - \mathbf{c}^T \hat{\mathbf{x}}_i) \quad (37)$$

$$\mathbf{\Omega}_i = \mathbf{A}_i \mathbf{\Omega}_{i-1} \mathbf{A}_i^T + \text{diag}(\mathbf{u}_{OU,i}) - \mathbf{\Theta}_i \mathbf{\Theta}_i^T / \Delta_{i-1} \quad (38)$$

$$u_{OU,ij} = \frac{\varsigma^2}{2\omega_j} \left(1 - e^{-(t_i - t_{i-1})\omega_j}\right) \quad (39)$$

$$\hat{y}_i = \mu + \mathbf{c}^T \hat{\mathbf{x}}_i \quad (40)$$

$$\Delta_i = \mathbf{c}^T \mathbf{\Omega}_i \mathbf{c} + v_i. \quad (41)$$

¹ State-space representations and the Kalman recursions are commonly used in time series analysis. A good introduction to these techniques is given by Brockwell & Davis (2002).

Here, \mathbf{c} and ω denote the M -dimensional vectors of mixing weights and characteristic frequencies, respectively, \mathbf{x}^T denotes the transpose of \mathbf{x} , and Equations (35)–(41) are only valid for $i > 1$. Recall that the M characteristic time scales are $\tau_1 = 1/\omega_1, \dots, \tau_M = 1/\omega_M$. Equation (30) can then be maximized to calculate maximum-likelihood estimates of \mathbf{c}, μ, ω , and ς , or used to perform Bayesian inference in combination with a prior distribution. Precise determination of the mixing weights will in general only be possible with the highest quality lightcurves, as the estimates will have a large uncertainty with high levels of correlation in their error distribution.

In practice, an additional constraint needs to be imposed on the norm of \mathbf{c} , as it is degenerate with ς . In this work we impose a unit squared norm constraint on the weights:

$$\|\mathbf{c}\|^2 = \sum_{i=1}^M c_i^2 = 1. \quad (42)$$

Under this normalization, the PSD at frequencies $\omega \gg \max\{\omega_1, \dots, \omega_M\}$ is

$$P(\omega) \sim \frac{\varsigma^2}{2\pi\omega^2}, \quad (43)$$

from which it is apparent that the amplitude of the high frequency PSD is proportional to ς^2 . Thus, ς not only gives rate at which variability power is injected into the stochastic process, but also defines the amplitude of variability at the highest frequencies. The amount of high frequency variability in a time interval $t_1 < t < t_2$ is given by the integral of Equation (43) over this time interval:

$$\text{Var}(t_1 < t < t_2) = \frac{\varsigma^2}{2\pi} (t_2 - t_1), \quad t_2 \ll 1/\omega_H. \quad (44)$$

So long as $M \ll N$, calculation of the likelihood via Equations (30)–(41) is much faster than direct calculation using the autocovariance matrix, $R_Y(\mathbf{t})$. In addition, we note that Equation (30) is only valid for Gaussian measurement errors, and therefore, one must have obtained a suitably high number of counts in order to use it for X-ray and gamma ray data. An extension to the low-count Poisson regime is beyond the scope of our current paper, but will be developed in future work (Kelly et al., in preparation).

Because we are primarily interested in bending power-law forms of the power spectrum, we use a mixed OU process which can accurately model these forms. We have found that the following weighting scheme on a regular grid in $\log \omega_j$ can provide a good approximation to a bending power-law with two breaks:

$$c_j = \omega_j^{1-\alpha/2} \left(\sum_{j=1}^M \omega_j^{2-\alpha} \right)^{-1/2} \quad (45)$$

$$\log \omega_j = \log \omega_L + \frac{j-1}{M-1} (\log \omega_H - \log \omega_L), \quad j = 1, \dots, M. \quad (46)$$

Here, the parameters of the process are $\mu, \varsigma, \omega_L, \omega_H$, and α . The mean of the process is μ , ς is the standard deviation of the driving noise, ω_H and ω_L are the high and low frequency breaks in the power spectrum, and α is

the slope of the power spectrum in the intermediate region. The power spectrum for the process defined by Equations (45)–(46) is flat for frequencies $\omega \lesssim \omega_L$, decays as $P(\omega) \propto 1/\omega^\alpha$ for $\omega_L \lesssim \omega \lesssim \omega_H$, and decays as $P(\omega) \propto 1/\omega^2$ for $\omega \gtrsim \omega_H$. We have experimented with different values of M , and find that values of $M \gtrsim 30$ are more than sufficient; there is little change in the power spectrum among values of $M \gtrsim 30$.

The likelihood function may be used to calculate a maximum-likelihood estimate. However, in order to get reliable estimates of the uncertainties on the mixed OU process parameters, we employ a Bayesian approach which calculates the posterior probability distribution of the parameters, given the observed lightcurve. The probability distribution of the parameters given the observed lightcurve is

$$p(\mathbf{c}, \omega, \mu, \varsigma | \mathbf{y}) \propto p(\mathbf{y} | \mathbf{c}, \omega, \mu, \varsigma) p(\mathbf{c}, \omega, \mu, \varsigma), \quad (47)$$

where the prior distribution is $p(\mathbf{c}, \omega, \mu, \varsigma)$. For the prior under the power-law weighting scheme, we fix the values of \mathbf{c} and ω to those in Equations (45) and (46), and assume a uniform prior on $-2 < \alpha < 0$, μ , and $\varsigma > 0$. We assume the following prior on the logarithm of the break frequencies:

$$\begin{aligned} p(\log \omega_L, \log \omega_H) &= p(\log \omega_H | \log \omega_L) p(\log \omega_L) \\ &= \frac{1}{\log \omega_{max} - \log \omega_L}, \quad \omega_{min} \leq \omega_L \leq \omega_H \leq \omega_{max}. \end{aligned} \quad (48)$$

Equation (48) is equivalent to placing a uniform prior on $\log \omega_L$ over the range $\omega_{min} \leq \omega_L \leq \omega_{max}$ and a uniform prior on $\log \omega_H$ over the range $\omega_L \leq \omega_H \leq \omega_{max}$. The upper and lower limits on the characteristic time scales that we search for, $\tau_{max} = 1/\omega_{min}$ and $\tau_{min} = 1/\omega_{max}$, are chosen to be 10 times the length of the time series, and 1/10th the smallest time spacing in the time series. We use a Markov chain Monte Carlo (MCMC) algorithm to obtain random draws of the parameters from Equation (47).

4.2. Assessing the Quality of the Fit

We suggest two ways of assessing the quality of the mixed OU process in fitting the observed lightcurve. First, one should analyze the residuals to make sure that there are no systematic trends with time, and to ensure that there are no significant deviations from normality. If there are systematic trends with time, this may imply the existence of nonlinear effects. Define the standardized residuals as

$$\chi_i \equiv \frac{y_i - \hat{y}_i}{\Delta_i}. \quad (49)$$

Under the assumptions used to derive the likelihood function, the sequence of χ_i should follow a zero mean Gaussian white noise process with unit variance; i.e., there should be no systematic trends in $\{\chi_i\}$ with time and the distribution of the set of χ_i should be a Gaussian distribution with zero mean and variance equal to one. In practice, these assumptions are rarely true, although often the Gaussian likelihood approximation is adequate for estimating features in the power spectrum, such as characteristic time scales and the logarithmic slope of the power spectrum, so long as there are not many large outliers.

The second method for assessing the quality of the fit which should be employed is to assess how well the mixed OU process fits the observed periodogram. This is similar in spirit to the Monte Carlo method of Uttley et al. (2002), and enables one to assess whether there are features on different time scales which the mixed OU process does not fit well, as such discrepancies may be difficult to analyze in the lightcurve residual plot. First, one should calculate the periodogram of the observed lightcurve. Then, one can simulate a lightcurve having the same time sampling as the observed lightcurve for each of the mixed OU process parameters obtained from the MCMC sampler. Alternatively, one could also just use the maximum-likelihood estimate, but simulating lightcurves for each of the MCMC random draws also incorporates our uncertainty in the model parameters. Then, for each simulated lightcurve one calculates a periodogram. These periodograms can then be compared with the periodogram for the actual observed lightcurve to assess whether there are any time scales where the mixed OU stochastic process provides a poor fit.

5. APPLICATION TO BLACK HOLE LIGHTCURVES

In order to illustrate our method, and to investigate its effectiveness, we applied it to three different data sets. The first is an X-ray lightcurve of the galactic black hole Cygnus X-1 in the low/hard state. For this object, the data is of high enough quality to clearly see two breaks in the power spectrum. The second data set is the sample of local AGN with long-term RXTE data studied by Sobolewska & Papadakis (2009), supplemented with XMM lightcurves when available. This sample of objects is well-studied, and broken power-law models have been estimated and reported by many authors. Both of these data sets provide a good test for our statistical model, as it allows us to compare it with other well-established methods. The third data set consists of optical lightcurves of AGN from the MACHO survey and the AGN Watch sample, taken from Kelly et al. (2009). Kelly et al. (2009) analyzed these objects using only a single OU process, which is not as flexible as the mixed OU process. We exclude the lightcurves from the Givon et al. (1999) sample used by Kelly et al. (2009), as they are not as well sampled as the MACHO and AGN Watch sample.

5.1. Application to Cygnus X-1

We used an archival RXTE observation of Cygnus X-1 from Oct 23, 1996 (Obs ID 10241-01-01-000), which Nowak et al. (1999) have analyzed and identify as a hard-state lightcurve. We extracted the binned PCA lightcurve, using all channels, with the standard reduction routines. The lightcurve spanned ~ 28 ksec and was binned in 0.01 sec intervals. The PSD for this observation is shown in Figure 2, where we have subtracted off the Poisson noise level. We modeled the PSD using a mixture of 32 OU processes, treating the weights as free parameters on a fixed logarithmic grid in the characteristic frequencies, ω_j ; the maximum and minimum values of ω_j correspond to an order of magnitude shorter and longer than the minimum and maximum time spacing observed in the lightcurve.

Unlike for AGNs, the lightcurve has $\sim 1.5 \times 10^6$ data points, and computing the likelihood function is ex-

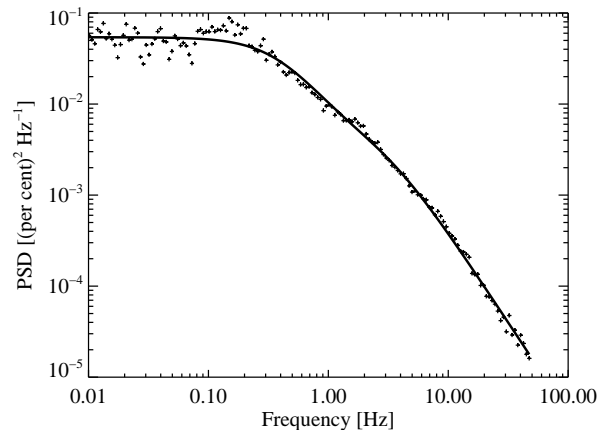


Figure 2. The observed PSD for an observation of Cygnus X-1 in the hard state (data points), compared with the best-fit PSD assuming the mixed OU process model (solid line). The mixed OU process model provides a good approximation to the observed PSD.

tremely computationally intensive. However, this large number of data points has the benefit that the PSD is very well determined. As a result, we do not estimate the parameters for the mixed OU process from the likelihood function of the lightcurve, but instead use least squares to fit the model PSD to the observed PSD. The result is also shown in Figure 2. It should be noted that we do not bin the lightcurve as an integer number times the time-resolution of the instrument mode, and thus some aliasing is introduced to the periodogram. However, we do not consider this a concern as aliasing is likely to be negligible for the low-frequencies used in the fit. As can be seen, the mixed OU process is able to provide a good approximation to the PSD for this observation of Cygnus X-1, although it is not a perfect fit. Further improvement could be obtained by making the characteristic frequencies of the individual OU processes free parameters as well; however, we do not do this as this would increase the number of free parameters to ≈ 60 – 70 , making the least-square optimization computationally difficult. We consider this approach of directly fitting the PSD satisfactory for Cygnus X-1, even if it is not as powerful as maximum-likelihood, as our primary goal in developing our method is to estimate features in the PSD, such as the break frequencies, from lightcurves that are of significantly poorer quality, for which high quality PSDs are not available. As such, we apply our model to Cygnus X-1 merely to illustrate that it provides a good approximation of the PSD.

5.2. AGN X-ray Lightcurves

5.2.1. Fitting Results

We applied our method to the X-ray lightcurves of 10 local AGN, studied recently by Sobolewska & Papadakis (2009). These objects have high quality lightcurves sampled over several decades in frequency, and have been extensively studied using Fourier-based techniques, making them a good sample for testing our method. The sample is summarized in Table 1, which includes the values obtained previously in the literature from Fourier-based techniques for the break frequency and logarithmic slope of the power spectra above the break fre-

quency. The 2–10 keV RXTE data is presented in Sobolewska & Papadakis (2009), and is important for studying the longer time scale behavior. In order to also study variations on time scales $\lesssim 1$ day, we included XMM lightcurves from the archives, when available. The XMM 2–10 keV background subtracted lightcurves were extracted using the standard routines of the XMM Scientific Analysis System, and were binned every 48 sec. Both the RXTE and XMM lightcurves were fit simultaneously. The XMM 2–10 keV count rates were converted to 2–10 keV fluxes using the 2–10 keV flux values calculated by de Marco et al. (2009), with the exception of NGC 5506, where we used the value calculated by Guainazzi et al. (2010). Sobolewska & Papadakis (2009) calculated the 2–10 keV luminosities based on the best fit spectral model to the 3–20 keV PCA data.

Our best fit parameters, as well as the 90% confidence intervals, are also summarized in Table 1. In general, our values are consistent with values previously obtained by other authors using the Fourier-based Monte Carlo method of Uttley et al. (2002), further validating our method. However, we obtain consistently smaller errors on the estimated parameters. This is likely primarily due to the facts that previous work treated the high frequency logarithmic slope of the power spectrum as a free parameter, while in our technique the high frequency end of the power law is assumed to decay as $1/f^2$, and that we work directly with the likelihood function.

In Figure 3 we show the posterior probability distributions of the characteristic time scales, logarithmic slope of the power spectrum between the break frequencies, and the total dispersion in the fractional variations, for two sources. The first source, MCG-6-30-15, represents some of the best time coverage that we have for our sample. The second source, ARK 564, is the only AGN with evidence for two break frequencies in its power spectrum, and is thought to be analogous to galactic black holes in the ‘very high state’ (McHardy et al. 2007); all other AGN in our sample are thought to be analogous to galactic black holes in the ‘high/soft’ state. We are able to confirm the existence of the two breaks in the power spectrum for ARK 564, corresponding to characteristic timescales of ~ 300 sec and ~ 2 days. However, for MCG-6-30-15, as with all other remaining AGN in our sample, there is still considerable probability on values of the longer time scale that are longer than the span of the lightcurve. As a result, we can only place a lower limit on the longer characteristic time scale, as we are only able to state with confidence that τ_L is not less than some value. For MCG-6-30-15, we find a lower limit of $\tau_L \gtrsim 37$ days.

We assessed the goodness of fit using the checks described in § 4.2. In general, the mixed OU process provided a good fit to the data, although the residuals exhibited some small deviations from the assumed Gaussian distribution. We do not consider this a concern, as it does not introduce a significant bias in the estimated parameters. As an example, in Figure 4 we compare the lightcurve of MCG-6-30-15 with the running average for the best-fitting mixed OU process. There do not appear to be any systematic trends in the residuals across the lightcurve. In addition, in Figure 5 we compare the periodogram of the lightcurve for MCG-6-30-15 with that expected from the best-fitting mixed OU process, after incorporating the uncertainty in the model parameters.

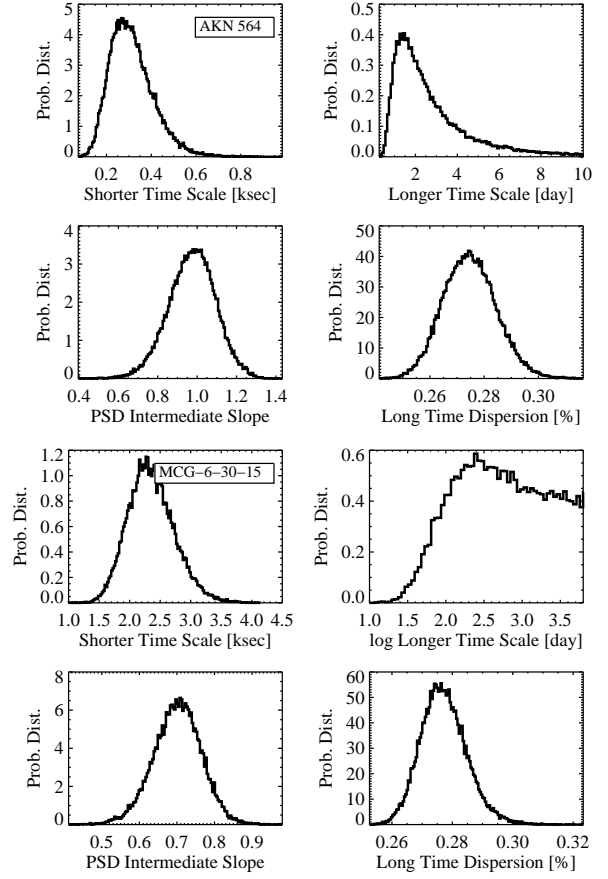


Figure 3. Posterior probability distribution for the short and long characteristic time scales, PSD slope between the break frequencies, and dispersion of the X-ray lightcurve for the AGN Akn 564 (left) and MCG-6-30-15 (right). For MCG-6-30-15 we are only able to place a lower limit on the longer characteristic time scale, or equivalently, a upper limit on the low-frequency break in the PSD.

We used the Lomb-Scargle periodogram for the RXTE data because of its irregular time sampling, while we used the standard discrete Fourier transform for the XMM data. The mixed OU process, with weights given by the bending power-law approximation (Eq. [45]), provides a good description of the X-ray lightcurve of MCG-6-30-15, being able to model the variability amplitude of luminosity fluctuations across a range of time scales.

As an additional check, we also used a flexible form for the mixed OU process, treating the values of the 32 weights as free parameters, but the break frequencies being fixed on a logarithmic grid in ω_j . This model provides more flexible modeling of the PSD, and we fit both the Akn 564 and MCG-6-30-15 X-ray lightcurves with it. The results are shown in Figure 6, where we compare the ‘flexible’ weighting with the power-law weighting. Note that here we have multiplied the PSDs by frequency, for easier comparison with previous work. We can still get good constraints on the PSD with the flexible weighting, although the uncertainties are now larger. For MCG-6-30-15, there does not appear to be a significant difference in the estimated PSD assuming the flexible weighting compared to the power-law weighting, although there may be some additional ‘wiggles’ in the PSD which the power-law weighting cannot fit. Similarly, the estimated

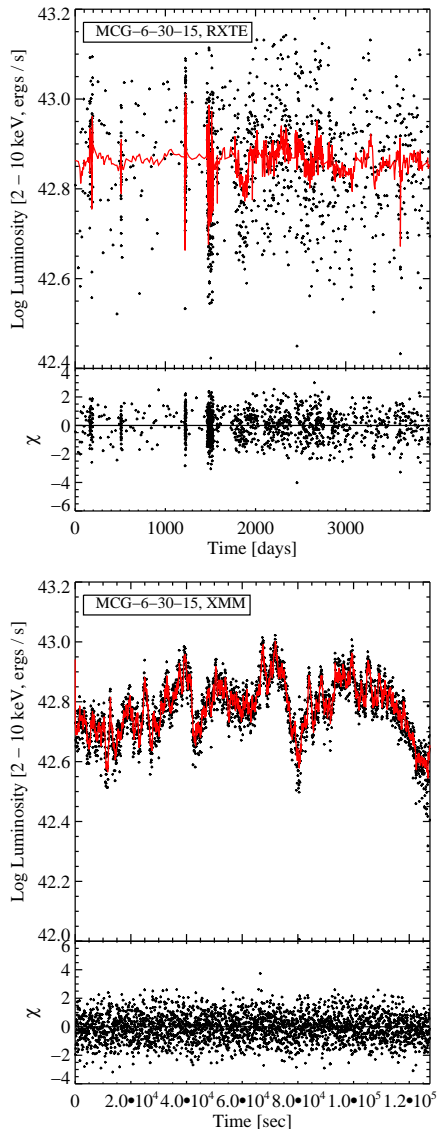


Figure 4. The observed RXTE (left) and XMM (right) lightcurves for MCG-6-30-15, compared with the running average of the best-fit mixed OU process model (red line) with power-law weights (Eq. [45]). The standardized residuals, given by Equation (49) are also shown in the lower panels. The mixed OU process is able to provide a good fit to the X-ray lightcurve for MCG-6-30-15, as evidenced by the apparent white noise character of the residuals.

PSD for Akn 564 assuming the flexible weighting displays some wiggles, suggesting that the simple bending power-law model is not able to capture all of the features of the PSD. Indeed, McHardy et al. (2007) find that a sum of Lorentzians provides a better fit to the PSD of Akn 564. Moreover, ‘wiggles’ and other deviations from a power-law PSD are seen in the X-ray PSDs of GBHs, and thus we might also expect them for AGN.

5.2.2. Comparison with Black Hole Mass

Sobolewska & Papadakis (2009) compiled black hole masses for the AGN, most of which are based on reverberation mapping (Peterson et al. 2004), and we use the values tabulated in Sobolewska & Papadakis (2009). The only exception is Mrk 766, which has a mass based on

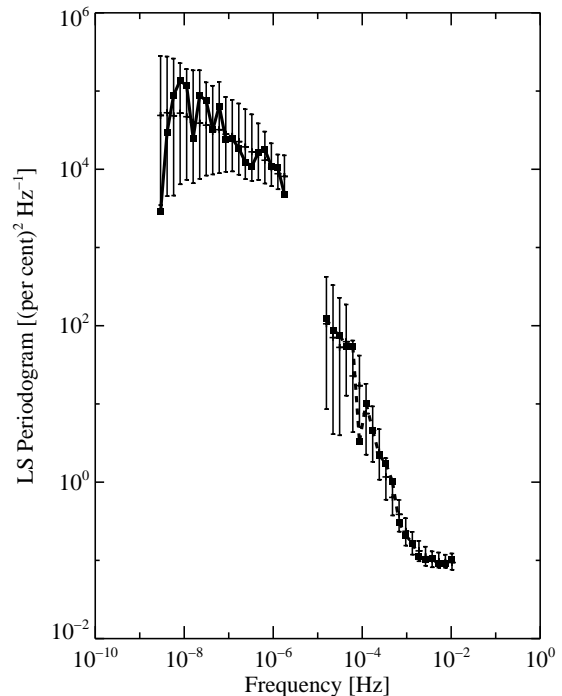


Figure 5. The Periodogram for the X-ray lightcurve of MCG-6-30-15 (connected squares) compared with the distribution of periodograms expected under the mixed OU process model with power-law weights (points with error bars). The error bars encompass 90% of the probability and represent the uncertainty in the expected observed periodogram due to uncertainty in the mixed OU process parameters, and due to variations in the sampled lightcurve due to its stochastic nature. The observed periodogram for MCG-6-30-15 is consistent with that expected for the Mixed OU process model, confirming that this model can accurately model the variability of the X-ray fluctuations of this source across a large range in time scales.

reverberation mapping calculated by Bentz et al. (2009). In Figure 7 we plot the characteristic time scale corresponding to the high frequency break, τ_H , as a function of black hole mass. We find a strong correlation between the two quantities, although this is not surprising as several authors have previously found a correlation based on direct PSD fitting of these same sources (e.g., Uttley & McHardy 2005; McHardy et al. 2006). However, using our statistical technique we obtain estimates for the break time scales for the two highest mass objects, Fairall 9 and NGC 5548, which previous work did not include as only lower limits on the break time scales were available. This correlation has typically been interpreted as being driven by a correlation between black hole mass and some relevant physical time scale in the X-ray emitting region, e.g., the viscous or thermal time scale, which corresponds to the suppression of fluctuations on time scales short compared to this characteristic time scale. However, based on the discussion in § 3, another, possibly related, interpretation is that the long time scale break corresponds to the characteristic time scale of the physical process driving the fluctuations, which increases with black hole mass, while the correlation between the short time scale break and black hole mass is caused by an increase in the characteristic spatial scale of the noise process driving the fluctuations with increasing black hole mass.

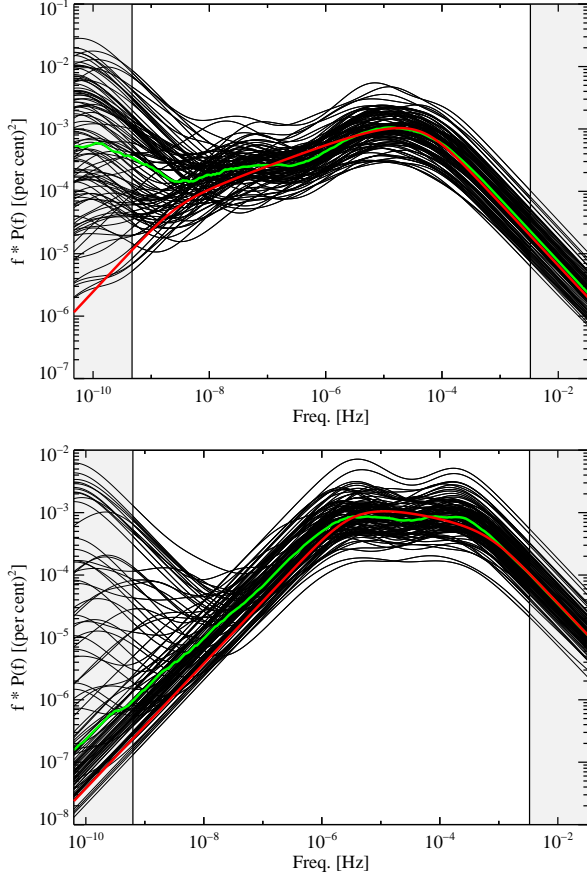


Figure 6. PSDs for MCG-6-30-15 (left) and Akn 564 (right) assuming the flexible weighting of the mixed OU process model. Here we have plotted $fP(f)$ for better comparison with other work. The thin black lines denote 100 random realizations of the PSD from its probability distribution, given the observed lightcurve, and the thick green lines denotes the median of the random realizations. The median value may be considered a ‘best-fit’ value of the PSD, and the spread of the black lines give a graphical representation of the uncertainty in the PSD; that probability that the PSD has a certain value may be estimated by counting the fraction of black lines that intersect that value. The thick red line denotes the best-fit PSD assuming the power-law weighting, and the shaded regions denote the areas of frequency space not probed by the observed lightcurve. While the bending power-law provides a reasonable approximation to the PSDs, both sources display additional ‘wiggles’ in the PSD that are not fit by the bending power-law model, similar to what is observed for GBHs.

We fit a linear relationship between $\log \tau_H$ and $\log M_{BH}$ using the Bayesian linear regression method of Kelly (2007), which accounts for the measurement errors in both $\log \tau_H$ and $\log M_{BH}$. It is especially important in this case to use a Bayesian method which incorporates the measurement errors because we only have 10 data points, and thus Bayesian methods are needed in order to accurately quantify the uncertainties. We find that on average

$$\tau_H = 3.00^{+4.57}_{-1.90} \left(\frac{M_{BH}}{10^7 M_\odot} \right)^{1.39 \pm 0.64} \text{ (ksec)} \quad (50)$$

where the errors are quoted at 90% confidence. We estimate the intrinsic scatter in τ_H at fixed M_{BH} to be ~ 0.6 dex. There is still potentially large intrinsic scatter in τ_H at fixed M_{BH} , which is likely due to scatter in the ac-

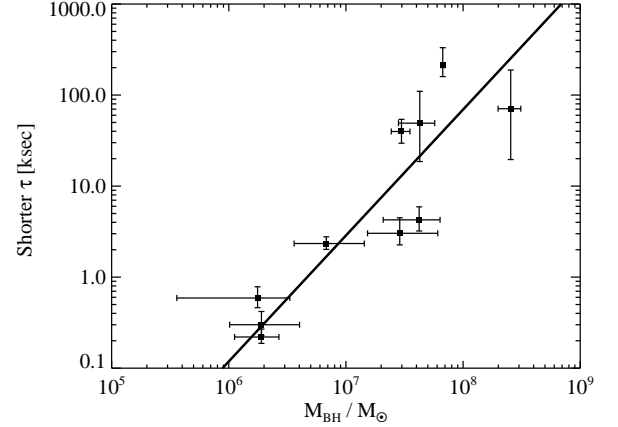


Figure 7. Dependence of characteristic time scale corresponding to the X-ray high frequency break on black hole mass. The error bars denote 68% confidence regions, and the solid line shows the best-fit linear relationship (Eq.[50]). Similar to previous work, we find a clear dependence of τ_H on M_{BH} .

cretion rates at fixed M_{BH} (e.g., McHardy et al. 2006); however, we stress that the estimate of the dispersion in the intrinsic scatter is highly uncertain, and more data is needed.

We also searched for correlations of M_{BH} with the PSD slope below the high frequency break α , amplitude of driving noise ς , and the total variability amplitude based on the mixed OU process model. We did not find any significant evidence for trends involving α or the total variability amplitude; however, we did find a highly significant anti-correlation between ς and M_{BH} , as shown in Figure 8. The trend is surprisingly tight, and implies that the fractional X-ray variations on time scales short compared to the high frequency break are weaker for AGN with more massive black holes (see Eq.[44]), or rather that the rate at which variability power is injected into the lightcurve decreases with increasing M_{BH} . Within the context of the stochastic linear diffusion model, this implies that the fractional amplitude of the driving noise field, which may be associated with MHD turbulence, decreases with M_{BH} . The Bayesian linear regression finds

$$\varsigma = 0.29^{+0.14}_{-0.08} \left(\frac{M_{BH}}{10^7 M_\odot} \right)^{-0.79 \pm 0.22} \text{ (per cent sec}^{-1/2}\text{)} \quad (51)$$

where the error are quoted at 90% confidence. We estimate the intrinsic scatter in ς at fixed M_{BH} to be ~ 0.2 dex.

This result is in agreement with previous work which has found an anti-correlation between the excess variance in the X-ray lightcurve and M_{BH} (e.g., Lu & Yu 2001; Papadakis 2004; Nikolajuk et al. 2004; O’Neill et al. 2005; Zhou et al. 2010). A similar anti-correlation between the rate at which variability power is injected into the lightcurve and black hole mass has also been found for AGN optical variations (KBS09). Czerny et al. (2001) find an anti-correlation between M_{BH} and the frequency at which the PSD reaches a reference value, which is consistent with an anti-correlation between M_{BH} and the amplitude of the high-frequency PSD. However, our result differs from most previous work in that we do not compute the variance over some range of time scales, di-

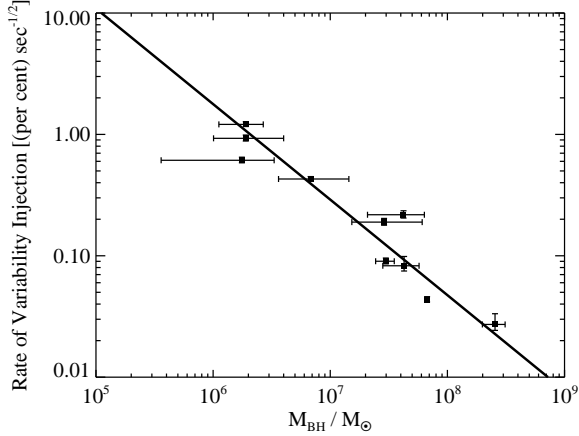


Figure 8. Dependence of ς on black hole mass; note that ς parameterizes the amplitude of the X-ray PSD on time scales short compared to the high frequency break, and is proportional to the amplitude of the driving noise field for the mixed OU process model. The error bars denote 68% confidence regions, and the solid line shows the best-fit linear relationship (Eq.[50]). There is a clear, very tight relationship between ς and M_{BH} .

rectly from the observed lightcurve, but rather we fit a parameter ς , which is the rate at which variability power is injected into the lightcurve. As shown in Equation (44), the parameter ς^2 is proportional to the short time scale variance, but is not strictly equal to it, as it does not depend on the time scales probed by the observed lightcurve. Indeed, under our adopted normalization for the mixed OU process weights (Eq.[42]), ς^2 essentially gives the normalization of the PSD on time scales short compared to the high frequency break. While the value of ς can be precisely determined in an unbiased manner using our statistical method, this is not the case for the observed variance in a lightcurve over some range of time scales. The observed variance in a lightcurve over some range of time scales is often a poor estimate of the actual time-averaged variance (Vaughan et al. 2003; O’Neill et al. 2005). The situation worsens if one is estimating the variance in the lightcurve using different time scales for different sources.

While we have shown that the amplitude of the high frequency variance is anti-correlated with M_{BH} , physically interpreting this correlation is difficult. Within the context of our mixed OU process model the anti-correlation implies that the amplitude of the driving noise field, and thus the rate at which variability power is injected into the lightcurve, decreases with increasing M_{BH} . However, this is also conditional on our adopted normalization for the mixing weights (Eq.[42]), and, as we stated earlier, the absolute values of the mixing weights are degenerate with ς^2 . Under our normalization, an anti-correlation between ς^2 and M_{BH} would be expected if the value of the PSD in between the break frequencies is independent of M_{BH} , assuming the PSD slope is equal to -1 , as ω_H is also anti-correlated with M_{BH} . Thus, the observed anti-correlation between ς^2 and M_{BH} could be a manifestation of the fact that the variability amplitude per frequency interval is constant between the break frequencies, but ω_H decreases with increasing M_{BH} . However, if it were true that the ς - M_{BH} anti-correlation is merely an artifact of the τ_H - M_{BH} correlation, then we

would expect the ς - M_{BH} relationship to have a slope of -0.5 . This is because the parameter ς^2 is proportional to the value of the PSD at fixed frequency, provided that $\omega \gg \omega_H$. If the value of $\omega P(\omega)$ is constant at the high frequency break, and if the break frequency scales as $\omega_H \propto M_{BH}^{-1}$, then we would expect that $\varsigma \propto M_{BH}^{-1/2}$. However, the dependence of ς on M_{BH} that we find in Equation (51, $\varsigma \propto M_{BH}^{-0.79}$) is steeper than that expected under this assumption of a scale-invariant PSD shape. This implies that the ς - M_{BH} anti-correlation is not simply an artifact of the τ_H - M_{BH} correlation, but is real.

The correlations between the high frequency break or ς and the black hole mass raise the possibility of using the X-ray lightcurve as an additional method for estimating black hole mass for AGN. It is thus of interest to assess the accuracy of the estimates derived from τ_H or ς . To do this, we also performed a linear regression of $\log M_{BH}$ on $\log \tau_H$ and $\log \varsigma$, respectively. Note that we cannot simply invert Equations (50) and (51), but need to perform the regression after switching the variables. Based on our results, mass estimates may be obtained as

$$\log(M_{BH}/M_\odot) = (6.75 \pm 0.20) + (0.60 \pm 0.14) \log(\tau_H/[1 \text{ ksec}])$$

$$\log(M_{BH}/M_\odot) = (6.36 \pm 0.19) - (1.20 \pm 0.18) \log(\varsigma/[(\text{per cent}) \text{ sec}^{-1/2}])$$

Here, unlike before, we have quoted the errors at 68% (1σ) confidence. The dispersion in $\log M_{BH}$ at fixed τ_H is ~ 0.4 dex, and the dispersion in $\log M_{BH}$ at fixed ς is ~ 0.2 dex, in agreement with the estimate of Zhou et al. (2010) when using the total high frequency variability amplitude. The probability distribution of the dispersion in mass at fixed τ_H and ς is shown in Figure 9; this quantity gives the precision in using these quantities as estimates of black hole mass. These results imply that mass estimates obtained from the high frequency break have similar accuracy to those obtained from the broad emission lines (~ 0.4 dex, Vestergaard & Peterson 2006), but are slightly less accurate than those obtained from the M_{BH} - σ relationship (~ 0.3 dex, Novak et al. 2006; Gültekin et al. 2009a). The mass estimates obtained from ς , on the other hand, appear to be the most accurate, on average, of all the single-observation techniques, at least for AGN, and have the advantage that the parameter ς can be determined from a single X-ray lightcurve with significantly higher precision than can the break frequency.

5.3. AGN Optical Lightcurves

Recent work has suggested that the optical lightcurves of AGN are well described by a single OU process (Kelly et al. 2009; Kozłowski et al. 2010; MacLeod et al. 2010a). The power spectrum for a single OU process becomes flat below the break frequency. It is worth investigating whether there is evidence for an intermediate region below the break frequency where the power spectrum falls off as $1/f^\alpha$, ($-2 < \alpha < 0$), similar to the X-ray lightcurves. We can do this by testing whether the optical lightcurves are better described by a mixed OU process, instead of a single OU process. We used a mixed OU process with weights given by Equation (45) to fit the high quality optical lightcurves of 63 AGN from the *MACHO* (Geha et al. 2003) and AGN Watch samples of Kelly et al. (2009). The 55 *MACHO* *R*- and *V*-band

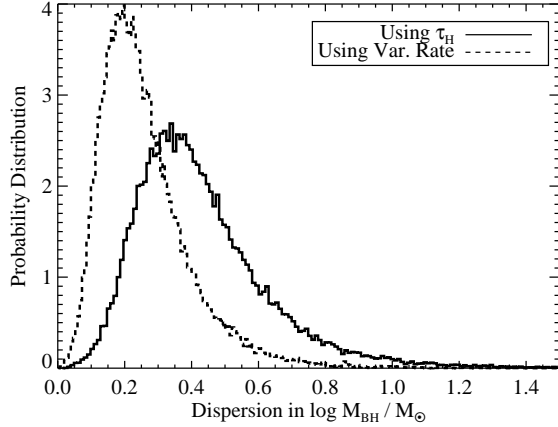


Figure 9. Probability distribution for the scatter in mass at a given τ_H (solid curve) or ς (dashed curve), given the 10 AGN in our data set. For comparison, mass estimates obtained from scaling relationships involving the broad emission lines and the host galaxy properties are ~ 0.4 and ~ 0.3 dex, respectively, implying that ς may give the most precise single-observation mass estimates.

lightcurves typically have seasonal time sampling of ~ 2 –10 days over ~ 7.5 years. The 8 Seyfert Galaxies from the AGN Watch database have optical lightcurves with varied time sampling and lengths, and were monitored for reverberation mapping. Further details of these samples are described in Kelly et al. (2009) and references therein.

We searched for objects for which the mixed OU process provided a better fit by finding those objects satisfying the union of the following two criteria:

- Most of the posterior probability for the ratio of break frequencies was found at values $\omega_H/\omega_L > 1$.
- Most of the posterior probability for the slope of the PSD between the two break frequencies was found at values $-2 < \alpha < 0$.

Note that these criteria essentially amount to finding the set of PSDs which do not reduce to the Lorentzian shape of the single OU process. For most sources, we did not find significant evidence that the mixed OU process provided a better fit to AGN optical variability than did a single OU process. Moreover, the characteristic time scales became significantly more uncertain under the mixed OU process model, most likely because we allowed the slope above the high frequency break to vary. However, we did find that for seven of the *MACHO* sources the mixed OU process provided a better fit to both the *R*- and *V*-band lightcurves. These sources had optical PSDs consistent with a single unbroken power-law with slope $-2 < \alpha < 0$, $P(f) \propto f^\alpha$, and thus no break frequencies were detected. There were a few additional objects for which either the *R*- or *V*-band PSD deviated from the Lorentzian shape of the OU process, but not both.

The seven objects for which both the *R*- and *V*-band lightcurves were better described by the mixed OU process are summarized in Table 2. We could not find anything unusual about these objects other than their timing properties. We also fit a flexible form of the mixed OU process to some of the better sampled optical lightcurves, treating the weights as free parameters on a fixed logarithmic grid for ω_j . We could not find any significant

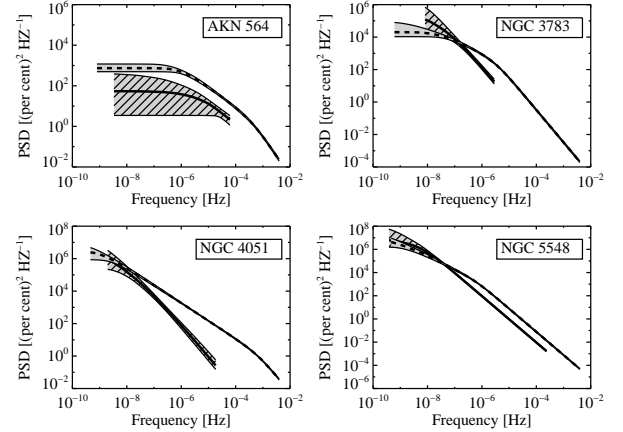


Figure 10. Comparison of the optical (solid line, diagonal line fill) and X-ray (dashed line, solid fill) PSDs for the four objects in our sample for which we have both good X-ray and optical lightcurves. The lines denote the best-fit PSDs and the shaded regions denote the 68% confidence regions for the PSDs, assuming the mixed OU process model with power-law weighting. In general, the optical PSDs fall off faster toward higher frequencies, implying that the short time scale variations are more suppressed in the optical lightcurves. However, the optical lightcurves appear to have more variability on longer time scale than the X-ray lightcurves, implying that the optical variations are not solely due to reprocessing of the X-ray emission. The only exception is Akn 564, which has a high accretion rate and is thought to be analogous to galactic black holes in the very high state.

evidence that the optical PSDs diverged from either a single power-law or Lorentzian PSD.

We have both optical and X-ray lightcurves for Akn 564, NGC 3783, NGC 4051, and NGC 5548, and it is worth comparing the two estimated PSDs for each source. In Figure 10 we compare the estimated optical and X-ray PSDs for each source assuming the mixed OU model with power law weighting. For all sources we subtracted off the host galaxy flux, where we used the values reported by Bentz et al. (2009) for NGC 3783, NGC 4051, and NGC 5548, and the value reported by Shemmer et al. (2001) for AKN 564. In general, the optical fluctuations are less variable than the X-ray fluctuations, except possibly on time scales $\gtrsim 100$ days. Furthermore, the optical PSDs fall off steeper toward high frequencies than the X-ray PSDs, and thus the short time scale optical fluctuations are more strongly suppressed relative to the X-ray fluctuations. These results are consistent with previous comparisons of optical and X-ray PSDs (e.g., Czerny et al. 1999, 2003; Uttley et al. 2003; Arévalo et al. 2008, 2009; Breedt et al. 2009, 2010).

One possible interpretation of these results is that the different PSDs represent how the different media in the two regions respond to a common driving process that is turbulent in both space and time, with the region emitting the optical photons more strongly suppressing the short-time scale noise fluctuations. This is consistent with the fact that ς is anti-correlated with M_{BH} for both the X-ray and optical lightcurves. For example, within the propagation class of models, this implies that while the source of the accretion rate perturbations may be the same, the optical emitting region more strongly suppresses the short time scale accretion rate perturbations, but when these perturbations reach the X-ray emitting region (i.e., the corona), which may also be subject to a

driving noise field, the short time scale fluctuations are not as strongly filtered as this medium is not as ‘stiff’. However, if the optical PSDs continue to rise above the X-ray PSDs at longer time scales, as it appears they do, then the total amplitude of variability in the optical fluctuations surpasses that in the X-ray fluctuations. This is a departure from the behavior seen in soft state GBH, where the disk emission is significantly less variable than the corona, suggesting a discrepancy between the spectral-timing properties of GBHs and AGN. In addition, larger optical variability amplitude than X-ray variability amplitude implies that either the source of the variations is different for the two emission regions, or that the power in the disturbances is somehow dissipated such that their variability amplitude has decreased by the time they reach the X-ray emitting region. However, the results also imply that all of the optical variability cannot be due to reprocessing of X-ray emission, as has been shown in previous work (e.g., Czerny et al. 1999, 2003; Uttley et al. 2003). The only possible exception appears to be Akn 564, where the X-ray variability amplitude is larger at all time scales. Akn 564 is noteworthy as it is the only AGN known to exhibit a second low-frequency break, and the additional X-ray variability may be due to an increase in the strength of the X-ray power-law component, such as is seen in GBH in the VHS.

6. SUMMARY

In this work we have developed a new model for the lightcurves of accreting black holes. The model is based on a mixture of Ornstein-Uhlenbeck stochastic processes and also happens to be the solution to the linear diffusion equation perturbed by a spatially correlated noise field. In essence, our model for quasar lightcurves may be thought of as a type of basis expansion, where the basis for the lightcurve is a set of independent stochastic processes. This allows flexible modeling of the PSD so long as $-2 \leq d \log P / d \log f \leq 0$ for all frequencies of interest, and we show that the mixed OU process provides a good approximation to the X-ray lightcurves of GBHs, and the optical and X-ray lightcurves of AGN. Our main results are

- The mixed OU process is the solution to the linear diffusion equation perturbed by a spatially correlated noise field, and thus the mixed OU process describes the evolution of viscous, thermal, or radiative perturbations due to a driving noise, to the extent that the viscous, thermal, or radiative response of the accretion flow follows a linear diffusion equation. Within this interpretation, the low frequency break in the PSD corresponds to the diffusion time scale in the outer region of the accretion flow, and the shape of the PSD above the low frequency break depends on the viscosity of the flow (or, more generally, the diffusion coefficient). If the noise field is spatially correlated, then an additional high frequency break in the PSD may exist at the frequency corresponding to the time it takes a perturbation traveling at the viscous speed to cross the characteristic spatial scale of the noise field.
- We derive the likelihood function of a lightcurve for the mixed OU process, given by Equations (30)–(41). This allows one to estimate the parameters of

the mixed OU process for an observed lightcurve, and equivalently the PSD, in a manner which is computationally efficient, unbiased by red noise leak and aliasing, and fully accounts for irregular sampling and measurement errors. If the parameters for a bending power-law are desired, then we also derive a form for the mixing weights which approximates a bending power-law, given by Equation (45).

- We show that the mixture of Lorentzians PSDs implied by the mixed OU process stochastic model is a good fit to the PSD of an observation of Cygnus X-1 in the hard state.
- We applied our mixed OU process model to the X-ray lightcurves of 10 well-studied local AGN and show that it provides a good description of their lightcurves, and we recover many of the PSD features which have been obtained previously from direct fitting of the observed PSDs. We use the estimated break frequencies to recover the correlation between time scale of the high frequency break and black hole mass seen previously with this sample; this includes new estimates of the high frequency time scales for Fairall 9 and NGC 5548, for which previously only upper limits were obtained.
- We find a significant anti-correlation between black hole mass and the amplitude of the driving noise fluctuations, ζ , which also parameterizes the amplitude of the high frequency PSD. The form of this correlation is similar to what has been observed in optical lightcurves (KBS09), suggesting that the origin of the optical and X-ray variability for AGN is at least partially shared. This correlation is even tighter than that between M_{BH} and the break frequency. Mass estimates obtained using ζ appear to have an uncertainty of ~ 0.2 dex, potentially making it the best single-observation mass estimator for AGN.
- We did not find significant evidence that most optical lightcurves of AGN deviated significantly from a single OU process, i.e., a Lorentzian PSD. However, we did find evidence that the optical lightcurves of 7 AGN in a sample of 55 AGN from the *MACHO* survey exhibited PSDs which were flatter than the $1/f^2$ shape seen in the majority of the sample, but the origin of this difference is unclear. These sources may exhibit flatter PSDs because we are seeing them on the $1/f^\alpha$ part of the PSD, i.e., the break time scales are shorter and longer than the minimum and maximum time scales probed by the lightcurves.
- We compare the optical and X-ray PSDs for Akn 564, NGC 3783, NGC 4051, and NGC 5548 and find that for the three NGC sources the short time scale fluctuations are more suppressed in the optical, but the long time scale fluctuations appear to be stronger in the optical. This implies that the total variability amplitude in the optical fluctuations is larger than that in the X-ray fluctuations, and thus the optical fluctuations cannot be

caused solely by reprocessing of X-ray emission. In addition, if both the optical and X-ray fluctuations are caused by inwardly propagating fluctuations in, say, the accretion rate, then some of the power in the fluctuations must be dissipated by the time they reach the X-ray emitting region. Akn 564, the only AGN believed to be in the very high accretion rate state, does not exhibit this behavior, and the optical fluctuations are always less variable than the X-ray fluctuations, at least over the range of time scales we probe.

We would like to thank Phil Uttley for helpful conversations, and Simon Vaughan, Christopher Kochanek, Chelsea MacLeod, and Eric Feigelson for looking over and commenting on an earlier version of this manuscript.

We would also like to thank the anonymous referee for a careful reading and detailed comments which improved the quality of this paper. BK acknowledges support by NASA through Hubble Fellowship grants #HF-01220.01 and #HF-51243.01 awarded by the Space Telescope Science Institute, which is operated by the Association of Universities for Research in Astronomy, Inc., for NASA, under contract NAS 5-26555. This research is funded in part by NASA contract NAS8-39073. Partial support for this work was provided by the *Chandra* grant GO8-9125A. This research has made use of data obtained from the High Energy Astrophysics Science Archive Research Center (HEASARC), provided by NASA's Goddard Space Flight Center. This research has also made use of the NASA/IPAC Extragalactic Database (NED) which is operated by the Jet Propulsion Laboratory, California Institute of Technology, under contract with the National Aeronautics and Space Administration.

APPENDIX

LÉVY PROCESSES

Lévy processes form a general set of processes that include Brownian motion and compound Poisson processes, both relevant in astrophysics. Basically, a stochastic process is a Lévy process if it has stationary and independent increments. Brownian motion, or rather the Wiener process, is a random walk process with a power spectrum that decays as $1/\omega^2$. A white noise process is the derivative of Brownian motion, and is a stochastic process with mean zero and a flat power spectrum; conversely, Brownian motion is the integral of white noise. A Brownian motion for the process driving the luminosity fluctuations might be considered a reasonable approximation if the input driving noise, $dW(t)$, has a decorrelation time scale short compared to the characteristic time scale of the luminosity fluctuations, therefore implying that $dW(t)$ resembles white noise. Alternatively, a compound Poisson process may be considered to describe the variability in luminosity caused by flares above an accretion disk. If the number of flares in a time interval follows a Poisson distribution, and the luminosities of the flares are randomly drawn from some other probability distribution, then the sum of the flare luminosities is a compound Poisson process. In general, most of the results from § 2 are valid for any Lévy process with zero mean and unit variance. The assumption that the driving noise, $dW(t)$, has zero mean and unit variance is not very restrictive, as μ and ς can always be rescaled to make this so.

CONTINUOUS MIXTURES OF ORNSTEIN-UHLENBECK PROCESSES

A continuous mixture of independent OU processes, denoted as $Y(t)$, may be obtained as

$$Y(t) = \mu + \int_0^\infty \int_0^\infty X(t, \omega_0, \varsigma) C(\omega_0, \varsigma) d\omega_0 d\varsigma \quad (\text{B1})$$

Here, $C(\omega_0, \varsigma)$ is a weighting function which describes how much a given OU process contributes to the mixture, and the notation $X(t, \omega_0, \varsigma)$ defines an infinite set of independent OU processes indexed by the value of ω_0 and ς ; we will refer to $C(\omega_0, \varsigma)$ as the ‘mixing function’. We assume that the individual OU processes have zero mean, and that the mean of the mixed OU process is μ . Some previous work has focused on the special case where $C(\omega_0, \varsigma)$ is a probability distribution (e.g., Iglói & Terdik 1999; Eliazar & Klafter 2009). In general, the process $Y(t)$ is not Markovian but stationary (Eliazar & Klafter 2009).

We are allowed considerable flexibility in modeling the lightcurve $Y(t)$ via the mixing function, and as an example we focus on the special case where $C(\omega_0, \varsigma)$ is a step function over some range of ω_0 . Specifically,

$$C(\omega_0, \varsigma) = \begin{cases} 1, & \omega_L \leq \omega_0 \leq \omega_H \\ 0, & \text{otherwise} \end{cases} \quad (\text{B2})$$

The autocovariance function and power spectrum can be calculated for this choice of mixing function using the formulae given in Eliazar & Klafter (2009). The autocovariance function is

$$R_Y(t) = \frac{\varsigma^2}{2} [E_1(t/\tau_L) - E_1(t/\tau_H)], \quad (\text{B3})$$

where $\tau_L = 1/\omega_L$ and $\tau_H = 1/\omega_H$ are the maximum and minimum characteristic time scales of the mixture, and $E_1(x)$ is an exponential integral of first order:

$$E_1(x) = \int_1^\infty \frac{\exp(-xy)}{y} dy, \quad x > 0. \quad (\text{B4})$$

The variance of the continuous mixed OU process, $Y(t)$, is calculated by taking the limit of Equation (B3) as $t \rightarrow 0$:

$$\text{Var}[Y(t)] = \lim_{t' \rightarrow 0} R_Y(t') = \frac{\zeta^2}{2} \ln \left(\frac{\tau_L}{\tau_H} \right). \quad (\text{B5})$$

Because the individual OU processes involved in the mixture are assumed to have zero mean, the mean of $Y(t)$ is μ .

The power spectrum for the continuous mixed OU process with weighting function given by Equation (B2) is

$$P_Y(\omega) = \frac{\zeta^2}{2\pi\omega} \left[\tan^{-1} \left(\frac{\omega_H}{\omega} \right) - \tan^{-1} \left(\frac{\omega_L}{\omega} \right) \right]. \quad (\text{B6})$$

Three regions are of interest,

$$P_Y(\omega) \sim \begin{cases} \zeta^2(\tau_L - \tau_H)/2, & \omega \ll \omega_L \\ 1/\omega, & \omega_L \ll \omega \ll \omega_H \\ 1/\omega^2, & \omega \gg \omega_H \end{cases}. \quad (\text{B7})$$

Therefore, the mixed OU process resembles white noise on time scales $\delta t \gg \tau_L$, ‘pink’ or ‘flicker’ noise on time scales $\tau_H \ll \delta t \ll \tau_L$, and red noise on time scale $\delta t \ll \tau_H$. For a lightcurve that follows a mixed OU process, τ_L represents the maximum time scale on which $Y(t)$ is correlated; on time scales longer than τ_L the lightcurve ‘forgets’ about its previous behavior.

We can also formulate a mixed OU process with common driving noise. This process was studied by Eliazar & Klafter (2009). Physically, we might expect this type of process to arise if, for example, the fluctuations in the optical lightcurve were the result of reprocessing due to a common source which irradiates a range of radii, with the reprocessing time scales increasing with increasing radii. Denote this type of mixed OU process as $\tilde{Y}(t)$. In this case, the power spectrum using the mixing function defined by Equation (B2) is

$$P_{\tilde{Y}}(\omega) = \frac{\zeta^2}{8\pi} \left[\ln \left(\frac{\omega^2 + \omega_H^2}{\omega^2 + \omega_L^2} \right) \right]^2 + \frac{\zeta^2}{2\pi} \left[\tan^{-1} \left(\frac{\omega_H}{\omega} \right) - \tan^{-1} \left(\frac{\omega_L}{\omega} \right) \right]^2. \quad (\text{B8})$$

The mixed OU process with common driving noise exhibits less long-time scale variations than does the mixed OU process with independent driving noise, due to the correlation in the processes created by a common driving noise.

REFERENCES

- Arévalo, P., Papadakis, I. E., Uttley, P., McHardy, I. M., & Brinkmann, W. 2006, MNRAS, 372, 401
 Arévalo, P., & Uttley, P. 2006, MNRAS, 367, 801
 Arévalo, P., Uttley, P., Kaspi, S., Breedt, E., Lira, P., & McHardy, I. M. 2008, MNRAS, 389, 1479
 Arévalo, P., Uttley, P., Lira, P., Breedt, E., McHardy, I. M., & Churazov, E. 2009, MNRAS, 397, 2004
 Armitage, P. J., & Reynolds, C. S. 2003, MNRAS, 341, 1041
 Belloni, T. M. 2010, Lecture Notes in Physics, Berlin Springer Verlag, 794, 53
 Belloni, T., Klein-Wolt, M., Méndez, M., van der Klis, M., & van Paradijs, J. 2000, A&A, 355, 271
 Bentz, M. C., et al. 2009, ApJ, 705, 199
 Bian, W., & Zhao, Y. 2003, MNRAS, 343, 164
 Bower, R. G., Benson, A. J., Malbon, R., Helly, J. C., Frenk, C. S., Baugh, C. M., Cole, S., & Lacey, C. G. 2006, MNRAS, 370, 645
 Breedt, E., et al. 2009, MNRAS, 394, 427
 Breedt, E., et al. 2010, MNRAS, 403, 605
 Brockwell, P. J., & Davis, R. A. 2002 Introduction to Time Series and Forecasting (2nd Ed.; New York, NY: Springer)
 Butler, N. R., & Bloom, J. S. 2010, submitted to ApJ(arXiv:1008.3143)
 Chow, P.-L. 2007, Stochastic Partial Differential Equations (Boca Raton, FL:Chapman & Hall/CRC)
 Churazov, E., Gilfanov, M., & Revnivtsev, M. 2001, MNRAS, 321, 759
 Collier, S., & Peterson, B. M. 2001, ApJ, 555, 775
 Croton, D. J., et al. 2006, MNRAS, 365, 11
 Cui, W., Zhang, S. N., Chen, W., & Morgan, E. H. 1999, ApJ, 512, L43
 Czerny, B., Nikolaïuk, M., Piasecki, M., & Kuraszkiewicz, J. 2001, MNRAS, 325, 865
 Czerny, B., Nikolaïuk, M., Róžańska, A., Dumont, A.-M., Loska, Z., & Zycki, P. T. 2003, A&A, 412, 317
 Czerny, B., Schwarzenberg-Czerny, A., & Loska, Z. 1999, MNRAS, 303, 148
 Czerny, B., Siemiginowska, A., Janiuk, A., Nikiel-Wroczyński, B., & Stawarz, L. 2009, ApJ, 698, 840
 de Marco, B., Iwasawa, K., Cappi, M., Dadina, M., Tombesi, F., Ponti, G., Celotti, A., & Miniutti, G. 2009, A&A, 507, 159
 Done, C., & Gierliński, M. 2005, MNRAS, 364, 208
 Done, C., Gierliński, M., & Kubota, A. 2007, A&A Rev., 15, 1
 Done, C., Madejski, G. M., Mushotzky, R. F., Turner, T. J., Koyama, K., & Kunieda, H. 1992, ApJ, 400, 138
 Eliazar, I., & Klafter, J. 2009, Phys. Rev. E, 79, 021115
 Emmanoulopoulos, D., McHardy, I. M., & Uttley, P. 2010, MNRAS, 404, 931
 Falcke, H., Kording, E., & Markoff, S. 2004, A&A, 414, 895
 Fender, R. P. 2001, MNRAS, 322, 31
 Fender, R. P., Belloni, T. M., & Gallo, E. 2004, MNRAS, 355, 1105
 Frank, J., King, A., & Raine, D. 2002, Accretion Power in Astrophysics (3rd Edition; Cambridge, UK:Cambridge Univ. Press)
 Gallo, L. C. 2006, MNRAS, 368, 479
 Gardiner, C. W. 2004, Handbook of Stochastic Methods (3rd Edition; Berlin:Springer-Verlag)
 Geha, M., et al. 2003, AJ, 125, 1
 Gierliński, M., Nikolaïuk, M., & Czerny, B. 2008, MNRAS, 383, 741

- Gillespie, D. T. 1996, *Am. J. Phys.*, 64, 225
- Giveon, U., Maoz, D., Kaspi, S., Netzer, H., & Smith, P. S. 1999, *MNRAS*, 306, 637
- Guainazzi, M., Bianchi, S., Matt, G., Dadina, M., Kaastra, J., Malzac, J., & Risaliti, G. 2010, *MNRAS*, 406, 2013
- Gültekin, K., et al. 2009, *ApJ*, 698, 198
- Gültekin, K., Cackett, E. M., Miller, J. M., Di Matteo, T., Markoff, S., & Richstone, D. O. 2009, *ApJ*, 706, 404
- Haardt, F., & Maraschi, L. 1991, *ApJ*, 380, L51
- Hawley, J. F., & Krolik, J. H. 2001, *ApJ*, 548, 348
- Ho, L. C. 1999, *ApJ*, 516, 672
- Horne, J. H., & Baliunas, S. L. 1986, *ApJ*, 302, 757
- Iglói, E., & Terdik, G., 1999, *Electron. J. Probab.* 4, 1
- Janiuk, A., & Czerny, B. 2007, *A&A*, 466, 793
- Janiuk, A., Czerny, B., Siemiginowska, A., & Szczerba, R. 2004, *ApJ*, 602, 595
- Kaspi, S., Maoz, D., Netzer, H., Peterson, B. M., Vestergaard, M., & Jannuzi, B. T. 2005, *ApJ*, 629, 61
- Kelly, B. C. 2007, *ApJ*, 665, 1489
- Kelly, B. C., Bechtold, J., & Siemiginowska, A. 2009, *ApJ*, 698, 895
- Kelly, B. C., Vestergaard, M., Fan, X., Hopkins, P., Hernquist, L., & Siemiginowska, A. 2010, in press at *ApJ*(arXiv:1006.3561)
- King, A. R., Pringle, J. E., West, R. G., & Livio, M. 2004, *MNRAS*, 348, 111
- Körding, E., Falcke, H., & Corbel, S. 2006, *A&A*, 456, 439
- Körding, E. G., Jester, S., & Fender, R. 2006, *MNRAS*, 372, 1366
- Kotov, O., Churazov, E., & Gilfanov, M. 2001, *MNRAS*, 327, 799
- Kozłowski, S., et al. 2010, *ApJ*, 708, 927
- Lightman, A. P., & Eardley, D. M. 1974, *ApJ*, 187, L1
- Lin, D. N. C., & Shields, G. A. 1986, *ApJ*, 305, 28
- Lomb, N. R. 1976, *Ap&SS*, 39, 447
- Lu, Y., & Yu, Q. 2001, *MNRAS*, 324, 653
- Lyubarskii, Y. E. 1997, *MNRAS*, 292, 679
- Maccarone, T. J. 2003, *A&A*, 409, 697
- MacLeod, C. L., et al. 2010, *ApJ*, 721, 1014
- MacLeod, C. L., et al. 2010, submitted to *ApJ*(arXiv:1009.2081)
- Markoff, S., Falcke, H., & Fender, R. 2001, *A&A*, 372, L25
- Markoff, S., Nowak, M. A., & Wilms, J. 2005, *ApJ*, 635, 1203
- Markowitz, A., et al. 2003, *ApJ*, 593, 96
- Mayer, M., & Pringle, J. E. 2006, *MNRAS*, 368, 379
- McAlary, C. W., McLaren, R. A., McGonagall, R. J., & Maza, J. 1983, *ApJS*, 52, 341
- McHardy, I. 2010, *Lecture Notes in Physics*, Berlin Springer Verlag, 794, 203
- McHardy, I. M., Arévalo, P., Uttley, P., Papadakis, I. E., Summons, D. P., Brinkmann, W., & Page, M. J. 2007, *MNRAS*, 382, 985
- McHardy, I. M., Gunn, K. F., Uttley, P., & Goad, M. R. 2005, *MNRAS*, 359, 1469
- McHardy, I. M., Koerding, E., Knigge, C., Uttley, P., & Fender, R. P. 2006, *Nature*, 444, 730
- McHardy, I. M., Papadakis, I. E., Uttley, P., Page, M. J., & Mason, K. O. 2004, *MNRAS*, 348, 783
- Merloni, A., Heinz, S., & di Matteo, T. 2003, *MNRAS*, 345, 1057
- Miller, L., Turner, T. J., Reeves, J. N., Lobban, A., Kraemer, S. B., & Crenshaw, D. M. 2010, *MNRAS*, 403, 196
- Misra, R., & Zdziarski, A. A. 2008, *MNRAS*, 387, 915
- Moscibrodzka, M., Proga, D., Czerny, B., & Siemiginowska, A. 2007, *A&A*, 474, 1
- Mueller, M., & Madejski, G. 2009, *ApJ*, 700, 243
- Nikolajuk, M., Papadakis, I. E., & Czerny, B. 2004, *MNRAS*, 350, L26
- Noble, S. C., & Krolik, J. H. 2009, *ApJ*, 703, 964
- Novak, G. S., Faber, S. M., & Dekel, A. 2006, *ApJ*, 637, 96
- Nowak, M. A., Vaughan, B. A., Wilms, J., Dove, J. B., & Begelman, M. C. 1999, *ApJ*, 510, 874
- O'Neill, P. M., Nandra, K., Papadakis, I. E., & Turner, T. J. 2005, *MNRAS*, 358, 1405
- Palma, W. 2007, *Long-Memory Time Series: Theory and Methods* (Hoboken, NJ: Wiley-Interscience)
- Papadakis, I. E. 2004, *MNRAS*, 348, 207
- Papadakis, I. E., Sobolewska, M., Arevalo, P., Markowitz, A., McHardy, I. M., Miller, L., Reeves, J. N., & Turner, T. J. 2009, *A&A*, 494, 905
- Pessah, M. E. 2007, *ApJ*, 655, 66
- Peterson, B. M., et al. 2004, *ApJ*, 613, 682
- Psaltis, D., & Norman, C. 2000, submitted to *ApJ*(arXiv:astro-ph/0001391)
- Quataert, E., Di Matteo, T., Narayan, R., & Ho, L. C. 1999, *ApJ*, 525, L89
- Remillard, R. A., & McClintock, J. E. 2006, *ARA&A*, 44, 49
- Reynolds, C. S., & Miller, M. C. 2009, *ApJ*, 692, 869
- Richards, G. T., et al. 2001, *AJ*, 121, 2308
- Romano, P., et al. 2004, *ApJ*, 602, 635
- Rossi, S., Homan, J., Miller, J. M., & Belloni, T. 2004, *Nuclear Physics B Proceedings Supplements*, 132, 416
- Rybicki, G. B., & Press, W. H. 1992, *ApJ*, 398, 169
- Scargle, J. D. 1981, *ApJS*, 45, 1
- Scargle, J. D. 1982, *ApJ*, 263, 835
- Schnittman, J. D., Krolik, J. H., & Hawley, J. F. 2006, *ApJ*, 651, 1031
- Shakura, N. I., & Sunyaev, R. A. 1973, *A&A*, 24, 337
- Shakura, N. I., & Sunyaev, R. A. 1976, *MNRAS*, 175, 613
- Shapiro, S. L., Lightman, A. P., & Eardley, D. M. 1976, *ApJ*, 204, 187
- Shemmer, O., et al. 2001, *ApJ*, 561, 162
- Siemiginowska, A., & Czerny, B. 1989, *MNRAS*, 239, 289
- Siemiginowska, A., Czerny, B., & Kostyunin, V. 1996, *ApJ*, 458, 491
- Sijacki, D., Springel, V., di Matteo, T., & Hernquist, L. 2007, *MNRAS*, 380, 877
- Smith, R., & Vaughan, S. 2007, *MNRAS*, 375, 1479
- Sobolewska, M. A., Gierliński, M., & Siemiginowska, A. 2009, *MNRAS*, 394, 1640
- Sobolewska, M. A., & Papadakis, I. E. 2009, *MNRAS*, 399, 1597
- Sobolewska, M. A., Siemiginowska, A., & Gierliński, M. 2011, submitted to *MNRAS*

- Sobolewska, M. A., Życki, P. T. 2006, MNRAS, 370, 405
- Starling, R. L. C., Siemiginowska, A., Uttley, P., & Soria, R. 2004, MNRAS, 347, 67
- Strom, A. L., Siemiginowska, A., Gurwell, M. A., & Kelly, B. C. 2010, arXiv:1001.0806
- Summons, D. P., Arévalo, P., McHardy, I. M., Uttley, P., & Bhaskar, A. 2007, MNRAS, 378, 649
- Sunyaev, R. A., & Titarchuk, L. G. 1980, A&A, 86, 121
- Sunyaev, R. A., & Titarchuk, L. G. 1985, A&A, 143, 374
- Titarchuk, L., Shaposhnikov, N., & Arefiev, V. 2007, ApJ, 660, 556
- Trump, J. R., et al. 2009, ApJ, 700, 49
- Trump, J. R., et al. 2009, ApJ, 706, 797
- Ulrich, M.-H., Maraschi, L., & Urry, C. M. 1997, ARA&A, 35, 445
- Uttley, P., Edelson, R., McHardy, I. M., Peterson, B. M., & Markowitz, A. 2003, ApJ, 584, L53
- Uttley, P., & McHardy, I. M. 2001, MNRAS, 323, L26
- Uttley, P., McHardy, I. M., & Papadakis, I. E. 2002, MNRAS, 332, 231
- Uttley, P., & McHardy, I. M. 2005, MNRAS, 363, 586
- Uttley, P., McHardy, I. M., & Vaughan, S. 2005, MNRAS, 359, 345
- Vaughan, S. 2010, MNRAS, 402, 307
- Vaughan, S., Edelson, R., Warwick, R. S., & Uttley, P. 2003, MNRAS, 345, 1271
- Vaughan, S., & Fabian, A. C. 2003, MNRAS, 341, 496
- Vestergaard, M. 2004, ApJ, 601, 676
- Vestergaard, M., & Peterson, B. M. 2006, ApJ, 641, 689
- Vio, R., Andreani, P., & Biggs, A. 2010, in press at A&A(arXiv:1006.2473)
- Wilkinson, T., & Uttley, P. 2009, MNRAS, 397, 666
- Wood, K. S., Titarchuk, L., Ray, P. S., Wolff, M. T., Lovellette, M. N., & Bandyopadhyay, R. M. 2001, ApJ, 563, 246
- Yuan, F., Yu, Z., & Ho, L. C. 2009, ApJ, 703, 1034
- Zechmeister, M., Kürster, M. 2009, A&A, 496, 577
- Zhou, X.-L., Zhang, S.-N., Wang, D.-X., & Zhu, L. 2010, ApJ, 710, 16
- Zu, Y., Kochanek, C. S., & Peterson, B. M. 2010, submitted to ApJ(arXiv:1008.0641)

Table 1
AGN with X-ray Lightcurves Analyzed

Name	z	Lit. f_H^a Hz	Lit. PSD Slope ^b	Reference ^c	f_H^d Hz	PSD Slope ^e	τ_L^f day	τ_H^g ksec	10 ⁻
Fairall 9	0.047	$3.98^{+2.33}_{-2.40} \times 10^{-7}$	$1.10^{+1.1}_{-0.6}$	1	$2.25^{+154}_{-1.73} \times 10^{-6}$	$1.58^{+0.25}_{-0.27}$	> 211	$70.8^{+232}_{-70.0}$	
Akn 564	0.025	$2.4^{+2.3}_{-0.9} \times 10^{-3}$	$1.2^{+0.2}_{-0.1}$	2	$5.25^{+3.55}_{-2.04} \times 10^{-4}$	$0.98^{+0.19}_{-0.21}$	$2.27^{+7.39}_{-1.36}$	$0.30^{+0.19}_{-0.12}$	
Mrk 766	0.013	$5^{+1}_{-3} \times 10^{-4}$	1 ⁱ	7	$2.69^{+1.51}_{-0.94} \times 10^{-4}$	$0.96^{+0.10}_{-0.12}$	> 31.0	$0.59^{+0.32}_{-0.21}$	
NGC 4051	0.002	$2.4^{+13}_{-2.3} \times 10^{-4j}$	$1.1^{+0.1}_{-0.4}$	4	$7.18^{+2.62}_{-1.84} \times 10^{-4}$	$1.10^{+0.04}_{-0.04}$	> 246	$0.22^{+0.08}_{-0.06}$	
NGC 3227	0.004	$2.6^{+5.3}_{-2.3} \times 10^{-4}$	$1.0^{+0.2}_{-0.4}$	6	$3.73^{+2.51}_{-1.44} \times 10^{-5}$	$1.20^{+0.08}_{-0.08}$	> 287	$4.26^{+2.67}_{-1.72}$	
NGC 5548	0.017	$6.31^{+18.8}_{-5.05} \times 10^{-7}$	$1.15^{+0.50}_{-0.65}$	1	$7.51^{+8.18}_{-3.33} \times 10^{-7}$	$1.22^{+0.29}_{-0.25}$	> 221.6	212^{+169}_{-111}	
NGC 3783	0.010	$6.2^{+40.6}_{-5.6} \times 10^{-6}$	$0.8^{+0.5}_{-0.8}$	5	$4.00^{+3.24}_{-1.47} \times 10^{-6}$	$0.79^{+0.42}_{-0.30}$	> 12.6	$39.8^{+23.3}_{-17.8}$	
NGC 5506	0.006	$3.9^{+16}_{-3.8} \times 10^{-5}$	$1.0^{+0.2}_{-1.0}$	6	$5.25^{+4.27}_{-2.20} \times 10^{-5}$	$1.11^{+0.16}_{-0.15}$	> 18.4	$3.03^{+2.18}_{-1.36}$	
MCG-6-30-15	0.008	$6.0^{+10}_{-5} \times 10^{-5}$	$0.8^{+0.16}_{-0.4}$	3	$6.80^{+2.12}_{-1.52} \times 10^{-5}$	$0.70^{+0.10}_{-0.11}$	> 36.6	$2.34^{+0.69}_{-0.56}$	
NGC 3516	0.009	$2.00^{+3.01}_{-1.00} \times 10^{-6}$	$1.10^{+0.4}_{-0.3}$	1	$3.24^{+46.7}_{-2.17} \times 10^{-6}$	$1.21^{+0.42}_{-0.39}$	> 39.07	$49.1^{+99.1}_{-45.9}$	

References. — (1) Markowitz et al. 2003 (2) McHardy et al. 2007 (3) McHardy et al. 2005 (4) McHardy et al. 2004 (5) Summons et al. 2007 (6) Uttley & McHardy 2005 (7) Vaughan

Note. — Error bars denote 90% Confidence Intervals, except for values from Markowitz et al. (2003) and McHardy et al. (2007), who report errors at the 68% level. Lower limits on τ_L

^a The location of the high-frequency break previously reported in the literature.

^b The value of α , $P(\nu) \propto f^{-\alpha}$ in the intermediate region of the PSD, below the high-frequency break, previously reported in the literature.

^c The reference for the literature values of f_H and α .

^d The estimated value of the location of the high-frequency break, obtained using our Bayesian implementation of the mixture of OU processes model.

^e Same as the previous column, but for the PSD logarithmic slope below the high-frequency break.

^f The longer characteristic time scale of the lightcurve, corresponding to the low-frequency break.

^g The shorter characteristic time scale of the lightcurve, corresponding to the high-frequency break.

^h The fractional amplitude of the driving noise field for the mixed OU process. Since we have normalized the weights to have unit norm, ζ^2 is also proportional to the lightcurve fractional

ⁱ Vaughan & Fabian (2003) fixed the intermediate PSD logarithmic slope to $\alpha = 1$ for Mrk 766.

^j The values reported by McHardy et al. (2004) are for a sharply broken power-law, as the authors did not state confidence regions for the bending power-law PSD model.

Table 2
MACHO Sources with Optical Lightcurves that Deviate from a Lorentzian PSD

MACHO ID	RA (J2000)	Dec (J2000)	z	V-band PSD Slope ^a	R-band PSD Slope
2.5873.82	05 16 28.78	-68 37 02.38	0.46	$1.42^{+0.05}_{-0.06}$	$1.35^{+0.05}_{-0.06}$
9.5484.258	05 14 12.05	-70 20 25.64	2.32	$1.42^{+0.10}_{-0.10}$	$1.63^{+0.29}_{-1.40}$
13.5717.178	05 15 36.02	-70 54 01.65	1.66	$1.40^{+0.09}_{-0.10}$	$1.50^{+0.23}_{-0.20}$
68.10968.235	05 47 45.13	-67 45 5.745	0.39	$1.15^{+0.17}_{-0.31}$	$0.98^{+0.17}_{-0.30}$
69.12549.21	05 57 22.41	-67 13 22.16	0.14	$1.57^{+0.11}_{-0.12}$	$1.82^{+0.14}_{-0.21}$
70.11469.82	05 50 33.31	-66 36 52.96	0.08	$1.69^{+0.24}_{-1.30}$	$1.60^{+0.21}_{-0.22}$
82.8403.551	05 31 59.66	-69 19 51.12	0.15	$1.10^{+0.06}_{-0.11}$	$1.47^{+0.31}_{-0.86}$

Note. — Error bars denote 90% Confidence Intervals.

^a The value of α , $P(f) \propto 1/f^\alpha$.